Telomerase reverse transcriptase promotes cardiac muscle cell proliferation, hypertrophy, and survival

Hidemasa Oh*†, George E. Taffet†‡, Keith A. Youker†‡, Mark L. Entman†‡, Paul A. Overbeek§, Lloyd H. Michael†‡, and Michael D. Schneider*†‡§¶‖

*Center for Cardiovascular Development and the ‡DeBakey Heart Center Graduate Program in Cardiovascular Sciences, Departments of †Medicine, §Molecular and Cellular Biology, and ¶Molecular Physiology and Biophysics, Baylor College of Medicine, Houston, TX 77030

Edited by Robert A. Weinberg, Whitehead Institute for Biomedical Research, Cambridge, MA, and approved July 5, 2001 (received for review April 5, 2001)

Cardiac muscle regeneration after injury is limited by "irreversible" cell cycle exit. Telomere shortening is one postulated basis for replicative senescence, via down-regulation of telomerase reverse transcriptase (TERT); telomere dysfunction also is associated with greater sensitivity to apoptosis. Forced expression of TERT in cardiac muscle in mice was sufficient to rescue telomerase activity and telomere length. Initially, the ventricle was hypercellular, with increased myocyte density and DNA synthesis. By 12 wk, cell cycling subsided; instead, cell enlargement (hypertrophy) was seen, without fibrosis or impaired function. Likewise, viral delivery of TERT was sufficient for hypertrophy in cultured cardiac myocytes. The TERT virus and transgene also conferred protection from apoptosis, *in vitro* and *in vivo*. Hyperplasia, hypertrophy, and survival all required active TERT and were not seen with a catalytically inactive mutation. Thus, TERT can delay cell cycle exit in cardiac muscle, induce hypertrophy in postmitotic cells, and promote cardiac myocyte survival.

Irreversible cell cycle exit limits the restoration of pump function after myocardial infarction (cardiac cell death from ischemia or reperfusion injury) or after chronic myocyte loss to apoptosis in heart failure (1). Thus, apart from fundamental interests, mechanisms underlying cardiac cell cycle exit hold importance given the therapeutic potential of regenerative cardiac muscle growth. Terminal differentiation involves the retinoblastoma family of tumor-suppressor pocket proteins and cyclin-dependent protein kinases (Cdks) that modulate their function (2). Although the role of pocket proteins and Cdks has been substantiated in cardiac cell cycle control (1, 3, 4), neither suffices to explain and impose the timing of the postmitotic phenotype *in vivo*. The likely need for multiple activators acting in concert and the coexistence of multiple inhibitors together create a formidable barrier to ventricular myocyte proliferation beyond the immediate perinatal period.

One mechanism that can cooperate with these, and mediates replicative senescence in other systems, is down-regulation of telomerase reverse transcriptase (TERT) and the resulting loss of telomerase activity (5–8). The telomere is a specialized DNA-protein complex, in species with linear genomes, that prevents linear chromosome ends from being sensed as a DNA strand break, triggering growth arrest and other responses (7–10). In vertebrates, the telomere comprises a conserved TTAGGG repeat, in a large duplex loop that buries the 3′ end in a lariat structure (9). As a putative mitotic clock (5–8), cell division erodes the telomeric repeat because of incomplete replication of the distal 3′ strand (the "end-replication" problem). During active replicative growth, TERT utilizes an intrinsic RNA component (TERC) as template, to restore the repeat and maintain telomere length. Telomere repeat-binding factors (TRF) 1 and 2 stabilize the lariat structure (7); TRF2, especially, is important for telomeric signaling to DNA damage checkpoint controls (10). At least in yeast, telomeric signals also involve transcriptional silencing of genes positioned near the telomere (7).

In adult humans, telomerase activity is found predominantly in germ cells, tumor cells, and stem cells with limitless proliferative capacity, but not somatic cells that ultimately senesce. In adult mice, telomerase activity is more widespread in tissue-specific patterns that correspond to the potential for sustained proliferation (11). Failure to express TERT is the principal mechanism for low levels of telomerase activity seen with replicative senescence. Telomerase activity can be reconstituted by ectopic expression of TERT (5, 12); thus, the catalytic subunit ordinarily is limiting. In mouse embryonic stem cells, even hemizygosity for TERT leads to telomere erosion (13). However, prolongation of cell lifespan can require other alterations in addition to TERT.

The need for whole-animal studies of telomerase function is underscored by discrepancies in long-term cell culture, used to model replicative senescence (8), plus differences among species in telomere biology (8, 14). The role of telomerase in mice has been questioned, in part because telomere length is greater in *Mus musculus* than in wild-derived species (11) or humans. Nevertheless, essential roles have been shown for mice, especially in highly proliferative organs, aging, and pathophysiological settings with high cell turnover (14). Of note, defects in mice lacking the RNA component of telomerase involve apoptosis, not just proliferation defects (14, 15), and telomerase may protect cells against at least some causes of programmed cell death (16).

Given that telomerase activity and TERT expression are lacking or are markedly decreased in the adult heart (17, 18), we postulated that preventing the down-regulation of TERT might delay or prevent the loss of telomerase activity and, if so, delay or prevent ventricular myocytes' exit from the cell cycle. To test this, exogenous TERT was forcibly expressed in mouse myocardium. TERT maintained telomerase activity in the adult heart and delayed ventricular myocytes' exit from the cell cycle in the first month after birth. Less expectedly, cardiac myocyte enlargement (hypertrophy) was provoked at later ages, without mechanical dysfunction or fibrosis as initiating factors. Hypertrophy also was elicited by TERT in cultured cardiac myocytes after viral gene transfer, suggesting additional functions of TERT beyond those reported to date. Consistent with other evidence for a cytoprotective effect of telomerase, TERT conferred protection from cardiac myocyte apoptosis. All three functions—delayed cell cycle exit, hypertrophy, and survival—required active TERT and were not evoked by a catalytically defective mutation.

Materials and Methods

Northern Blot Analysis. Twenty μg aliquots of cardiac RNA were size-fractionated in agarose/formaldehyde gels and transferred

This paper was submitted directly (Track II) to the PNAS office.

Abbreviations: ANF, atrial natriuretic factor; Cdk, cyclin-dependent kinase; MHC, myosin heavy chain; TERT, telomerase reverse transcriptase; TRAP, telomeric repeat amplification protocol; TRF, telomere repeat-binding factor.

‖To whom reprint requests should be addressed at: Baylor College of Medicine, One Baylor Plaza, Room 506C, Houston, TX 77030. E-mail: michaels@bcm.tmc.edu.

The publication costs of this article were defrayed in part by page charge payment. This article must therefore be hereby marked "*advertisement*" in accordance with 18 U.S.C. §1734 solely to indicate this fact.

www.pnas.org/cgi/doi/10.1073/pnas.191169098

to Hybond-N^+ membranes (Amersham Pharmacia Biotech). TERT, atrial natriuretic factor (ANF), myosin heavy chain (MHC), c-myc, and glyceraldehyde-3-phosphate dehydrogenase (GAPDH) probes were amplified by reverse transcription (RT)-PCR (19–21). Other probes were amplified by PCR, using the following primers: catalytic subunit of DNA-dependent protein kinase (DNA-PKcs), forward 5′-ATCAGAAGGTCTAAGGCTGGAAT-3′, reverse 5′-CGTACGGTGTTGGCTACTGC-3′; Ku70, forward 5′-GAGCATCCAGTGTATCCAGA-3′ and reverse 5′-CAGCATGATCCTCTTGTGAC-3′; Ku80, forward 5′-TCACAGTGTGCAGACACCTG-3′ and reverse 5′-AACTGCAGAGAGATGCCAGA-3′; TRF1, forward 5′-CATGGACTACACAGACTTAC-3′ and reverse 5′-ATCTGGCCTATCCTTAGACG-3′; and TRF2, forward 5′-TGTCTGTCGCGCATTGAAGA-3′ and reverse 5′-GCTGGAAGACCTCATAGGAA-3′.

Telomerase Activity. Telomerase activity was measured by a modified telomeric repeat amplification protocol (TRAP; TRAPeze; Intergen, Purchase, NY; ref. 22), using 1 μg of cell or tissue extract, PCR amplification for 28 cycles, and nondenaturing PAGE.

Telomere Length. Ten μg aliquots of cardiac DNA were digested with *Rsa*I, which yields 25–30-kbp telomeric fragments in mice (23), fractionated by 0.5% agarose gel electrophoresis, and transferred to Hybond-N^+ membranes. Hybridization was performed by using a ^{32}P-labeled $(TTAGGG)_4$ telomeric probe (24).

Generation of Active and Inactive TERT Transgenic Mice. The cardiac-specific TERT transgene was constructed using the human TERT coding sequence from pGRN145 (25), cloned 3′ to the 5.5-kbp mouse αMHC promoter (26) and 5′ to the human growth hormone (GH) polyadenylation sequence. Catalytically inactive TERT cDNA was produced by site-directed mutagenesis (aspartic acid to alanine at codon 868; D868A). Expression cassettes were released with *Kpn*I and *Not*I, and microinjected into the pronuclei of fertilized FVB/N oocytes. Tail DNA from 3-wk-old mice was subjected to Southern or dot blot analysis with full-length αMHC-TERT and αMHC-D868A.

Western Blot and Immune Complex Kinase Assays. Abs against TERT, Cdks, p70 S6K, JNK1, and ERK1/2 were from Santa Cruz Biotechnology. Abs for Akt, p38, and phosphorylated proteins were from New England Biolabs. Fifty μg aliquots were size-fractionated by SDS/PAGE and transferred to Immobilon-P membranes (Millipore). Membranes were incubated with primary Abs (1:500–1,000) then horseradish peroxidase-conjugated second Abs. Protein expression was visualized with enhanced chemiluminescence reagents (Amersham Pharmacia Biotech). Immune complex assays for Cdk activity were performed as described (3).

Cardiac Function and Structure. Transgenic animals and littermate controls underwent M-mode and Doppler echocardiography (27, 28). For histology, hearts were perfused with PBS followed by 10% (vol/vol) buffered formalin and embedded in paraffin. Myocardium was sectioned parallel to the plane of the atrioventricular valves at the level of the papillary muscles and was stained with hematoxylin and eosin or Sirius red.

Immunofluorescence Microscopy. Laminin staining was performed by using rabbit primary Ab (1:100; Sigma) and FITC-conjugated Ab to rabbit IgG (Molecular Probes). Nuclei were stained with 2 μg/ml of 4′,6-diamidino-2-phenylindole (DAPI). Images were captured with a Zeiss Axioplan 2 epifluorescence microscope. Myocyte diameter was measured by using the transnuclear width of random myocytes in cross-section at the papillary muscle level ($\geq$300 myocytes, using 2 hearts from each of 2 lines, by 2 blinded observers; ref. 29).

For phosphorylated histone H3, sections were digested with 0.05% trypsin and incubated with Abs to the Ser-10 phosphopeptide (1:1,000; Upstate Biotechnology, Lake Placid, NY; ref. 30) and sarcomeric MHC (1 μg/ml; MF20; University of Iowa Hybridoma Bank), then FITC- and Texas-red-conjugated Abs to rabbit and mouse IgG. BrdUrd (0.1 mg/g body weight) was administered i.p. 3 h before euthanasia and was detected with FITC-conjugated primary Ab (Roche Molecular Biochemicals).

Flow Cytometry. Ventricular myocytes were isolated by perfusion with 0.17% type I collagenase (CL1; Worthington; ref. 4). For each assay, 1×10^6 cells were fixed, labeled with FITC-MF20 and propidium iodide (PI) in the presence of RNaseA, and analyzed by two-color flow cytometry (3), using MODFIT 2.0 (Verity, Topsham, ME). DNA histograms were derived from the authenticated cardiac myocytes.

Cardiac Myocyte Culture and Adenoviral Gene Transfer. Ventricular myocytes from 2-day-old Sprague–Dawley rats were purified as described (3). Wild-type and catalytically inactive human TERT cDNAs were subcloned into pAdTrack-cytomegalovirus (CMV) and pShuttle-CMV (provided by Bert Vogelstein, Johns Hopkins Oncology Center, Baltimore), i.e., with and without coexpression of green fluorescent protein (GFP). Cardiac myocytes (10^6 cells per 60-mm dish) were infected for 6 h at 20 plaque-forming units per cell with adenovirus encoding wild-type TERT, D868A TERT, or the empty vector, and then were cultured for 24 h in serum-free medium, except where indicated. Infection efficiency was 100%, determined by coexpression of GFP or immunostaining for exogenous TERT.

Apoptosis. For cell culture, nucleosomal DNA fragmentation was monitored by electrophoresis in 1.5% agarose (31), and cell viability was monitored by trypan blue exclusion.

Ligation of the left anterior descending coronary artery was performed as described (28). The prevalence of myocyte apoptosis in the area perfused by the affected vessel was determined after 6 h of ischemia, using the *in situ* ligase reaction (32), which may be more specific than nick end-labeling for apoptotic strand breaks, especially when necrosis coexists (28). Twenty-four hours after ligation, the areas of infarction and ischemic risk were determined by using 1.5% triphenyltetrazolium chloride (TTC) staining and 1% Evan blue perfusion (28).

Statistical Analyses. Data are reported as the mean $\pm$ SE. Comparisons were analyzed by ANOVA and Scheffe's test, using a significance level of $P < 0.05$.

Results

Telomerase Activity, Telomere Length, and TERT Gene Expression Are Developmentally Regulated in Mouse Myocardium. Measured by the TRAP assay (22), telomerase activity was readily detected in embryonic (E16.5) and neonatal (2-day) mouse myocardium, with little or none in adult (8-wk) cardiac tissue (Fig. 1*A*), as reported for the rat (17, 18). Pretreatment of extracts with RNaseA, to confirm that the amplified products are attributable to telomerase, prevented formation of the TRAP ladder. Telomerase activity was down-regulated >65% by day 2 after birth. Telomeric restriction fragments (24) were analyzed by Southern blotting of cardiac DNA (Fig. 1*B*). As expected from the TRAP assay, cardiac telomere fragments were largest in embryos, and shortened with age.

Consistent with the loss of telomerase activity and decreased telomere length, TERT mRNA was most prominent in embryonic myocardium, was down-regulated 58% by day 2 after birth,

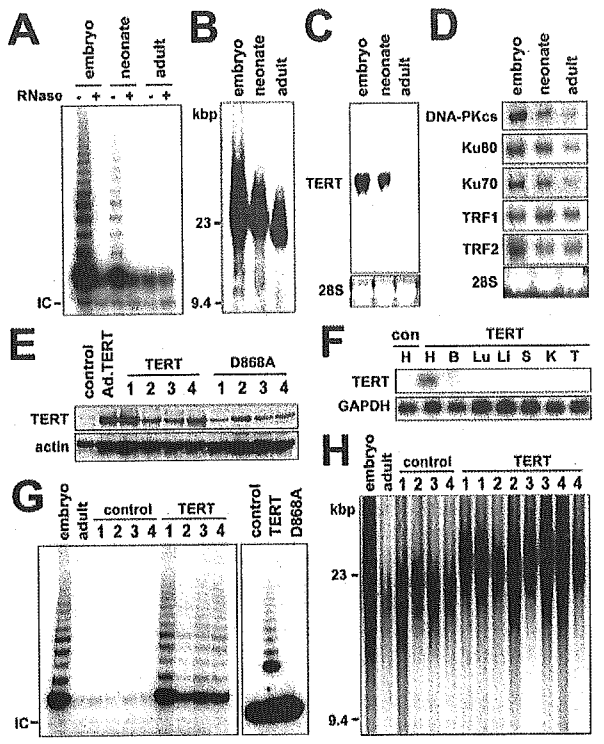

Fig. 1. Cardiac-specific overexpression of TERT restores telomerase activity and maintains telomere length. (*A*) Telomerase activity. Extracts from embryo (E16.5), neonate (day 2), and adult (8 wk) heart were assayed by a TRAP protocol, with (+) or without (−) RNaseA. IC, internal control template. (*B*) Telomere length. DNA extracted from myocardium was analyzed by Southern blotting for the telomeric repeat. (*C* and *D*) Northern blot analysis of TERT and telomerase-related factors during mouse cardiac development. Shown for comparison is 28S rRNA. (*E*) Western blot analysis of TERT transgene expression. TERT-infected cardiac myocytes were used as the positive control, and a nontransgenic littermate was used as the negative control. Total sarcomeric plus cytoplasmic actin is shown for comparison. (*F*) Northern blot analysis of TERT transgene expression. H, heart; B, brain; Lu, lung; Li, liver; S, spleen; K, kidney; T, testes; con, nontransgenic littermate. (*G*) Reconstitution of myocardial telomerase activity by TERT (*Left*) but not inactive TERT (D868A, *Right*). TRAP assays were performed as for *A*. (*H*) Restoration of telomere length in αMHC-TERT transgenic mice. In *E*, *G*, and *H*, numbers 1–4 denote 4 independent transgenic lines or the corresponding control littermates.

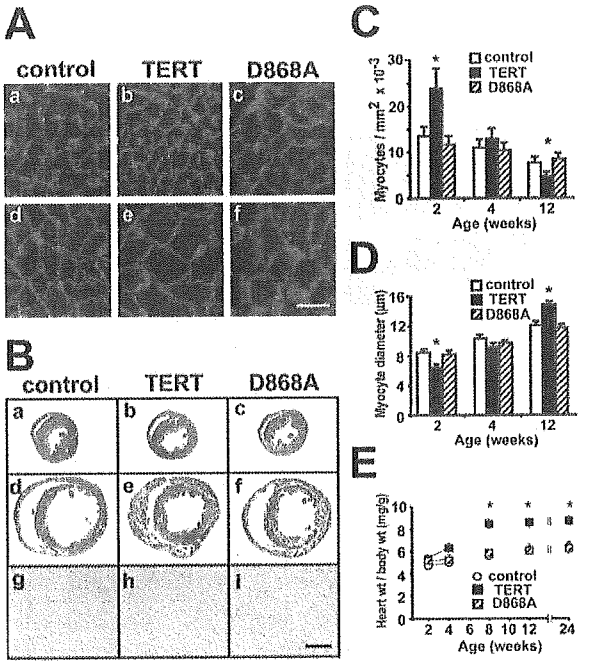

Fig. 2. TERT induces hypercellular myocardium, followed by cardiac hypertrophy. (*A*, *C*, and *D*) Laminin staining at 2 (*a–c*) and 12 (*d–f*) wk of age. TERT increased myocyte density at the younger age, but myocyte diameter at the older age. [Bar = 10 μm.] (*B*) Heart size, at 2 (*a–c*) and 12 (*d–f*) wk of age. Concentric biventricular hypertrophy was seen in 12-wk-old αMHC-TERT mice (*e*). *B g–i* show the lack of interstitial fibrosis in each genotype (Sirius red). [Bar = 1 mm, *a–f*; 20 μm, *g–i*.] (*E*) The heart weight per body weight ratio increased as a late response to TERT. *, $P < 0.05$ vs. transgene-negative littermates.

and was not detected in adult heart by Northern blotting (Fig. 1*C*). Other telomere-associated factors—the catalytic subunit of DNA-PK, its telomere-binding subunits (Ku70 and Ku80), and TRFs 1 and 2—were expressed even in postmitotic myocardium (Fig. 1*D*), as was the RNA component of telomerase (not shown), although the three components of DNA-PK were reduced in adult heart.

TERT Can Maintain Telomerase Activity and Telomere Length in the Adult Heart. The cardiac-specific αMHC promoter was used to direct the expression of wild-type human TERT vs. catalytically inactive TERT (D868A), and four founders were identified for each genotype. Transgene expression and tissue specificity were confirmed by Western blotting (Fig. 1 *E* and *F*). Telomerase activity was rescued in all four lines with wild-type TERT, but not by the D868A mutation at comparable levels (Fig. 1*G*). Southern blot analysis confirmed that telomere shortening in adult myocardium was suppressed by TERT (Fig. 1*H*).

TERT Can Delay Cardiac Myocyte Cell Cycle Exit, Then Leads to Late-Onset Cardiac Hypertrophy. To delineate cardiac myocyte boundaries, immunolabeling of laminin was performed (Fig. 2*A*, *C*, and *D*) (29). At 2 wk of age, myocyte density increased by two-thirds in TERT transgenic mice vs. controls, with myocyte diameter decreased, reciprocally. Similar conclusions were reached by using DAPI plus Ab to sarcomeric MHC (not shown). D868A transgenic mice were indistinguishable from transgene-negative animals. Given that cardiac dimensions and mass were unchanged at this age (Fig. 2 *B* and *E*), an increase in myocyte density suggests an increase in myocyte number (33).

Subsequently, the heart weight to body weight ratio increased, by one-third at 8 to 24 wk (Fig. 2*E*), with concentric hypertrophy in both ventricles (Fig. 2*B*). Myocyte diameter was likewise increased by TERT (12 wk; Fig. 2 *A*, *C*, and *D*), without tissue fibrosis (Fig. 2*B g–i*) or myocyte disarray (not shown). Echocardiography was performed to assess ventricular function (27), as hypertrophy could occur secondary to mechanical defects; no difference was seen in heart rate, ventricular performance, or chamber diameter (not shown). Although myocyte dropout from apoptosis also can be a cause of compensatory growth, no increase occurred in terminal deoxynucleotidyltransferase-mediated dUTP nick end-labeling (TUNEL)-positive cells (not shown). Thus, the early hyperplastic phenotype was followed by later hypertrophy, with neither cell loss nor discernible mechanical dysfunction as an explanation. Heart weight, wall thickness, and myocyte diameter were increased only by active TERT, not the inactive mutation.

Immunocytochemistry was performed for BrdUrd incorporation and histone H3 phosphorylation on Ser-10, markers of S

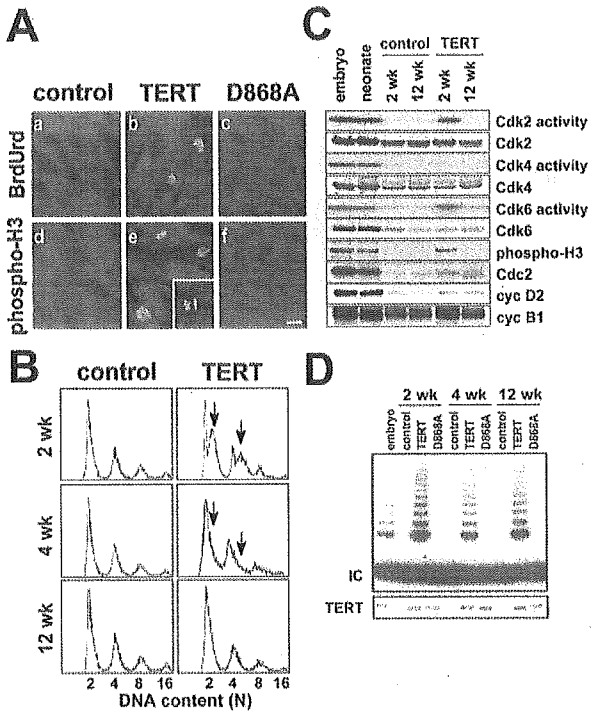

Fig. 3. Cardiac myocyte DNA synthesis and mitoses in αMHC-TERT transgenic mice. (*A*) Immunofluorescence detection of BrdUrd incorporation (green; *a–c*) and mitotic phosphorylation of histone H3 (green; *d–f*) in cardiac myocytes at 2 wk of age, identified with MF20 Ab to sarcomeric MHC (red). Neither BrdUrd incorporation nor histone H3 phosphorylation was detected in nontransgenic controls or D868A mice. A cardiac myocyte in late telophase is seen in *e* (*Inset*). [Bar = 10 μm.] (*B*) Dissociated cardiac myocytes were analyzed by flow cytometry. Arrows highlight the increase in DNA content by TERT. (*C*) TERT prolongs the activity of endogenous Cdk6, Cdk2, and Cdc2 in myocardium. Cdk2/4/6 activities were monitored by immune complex kinase assays, and Cdc2 activity was monitored by Ser-10 phosphorylation of histone H3. Western blots indicate an increase in cyc D2, cyc B1, and Cdc2 but not other Cdks. (*D*) The shift from hyperplasia to hypertrophy does not entail down-regulation of TERT expression (Western blot *Bottom*) or activity (TRAP assay *Top*).

phase and mitosis, respectively (Fig. 3*A*; Table 1). Neither was detected in age-matched littermate controls. Both BrdUrd incorporation and histone H3 phosphorylation were seen in αMHC-TERT ventricular myocytes, with a prevalence of ≈4,000 and 3,000/10^6, respectively, at 2 wk of age (Table 1). Similar results were confirmed in 3 additional lines (1,800–2,500/10^6 at 3 wk of age). Less frequently (125/10^6), myocyte nuclei suggestive of late telophase were seen (Fig. 3*A e Inset*). The prevalence of BrdUrd incorporation and histone H3 phosphorylation declined >50% by 4 wk of age; neither was detected at 12 wk of age, in either genotype. Thus, TERT delays, but (by itself) cannot prevent, cardiac cell cycle exit. All effects were specific to catalytically active TERT.

By using flow cytometry for DNA content (Fig. 3*B*), multiple peaks were seen with wild-type myocardium, as reported (4), corresponding to 2, 4, 8, or 16 haploid genomes per event. The prevalence of myocytes in S phase ($2 < n < 4$, plus $4 < n < 8$) was increased 3-fold by TERT at 2 wk, with a smaller shift to the right at 4 wk. Similar results were seen in two independent lines. By 12 wk, the distribution was no different from littermate controls.

To test whether TERT affected endogenous cell cycle regulators, myocardium was studied by Western blot analysis and immune complex kinase assays (Fig. 3*C*). Mitotic phosphorylation of histone H3 was sustained by TERT at 2 but not 12 wk, as was true by immunocytochemistry; this marker of Cdc2 function was accompanied by increased Cdc2 expression at the younger age. Cdk6 and Cdk2 activities increased 2- and 4-fold, respectively, at 2 wk, with no increase at 12 wk. Unlike Cdc2, these Cdks are ordinarily expressed even in adult myocardium, and their expression was not increased by TERT. Cyclins B1 and D2 were expressed at higher levels in αMHC-TERT myocardium at 2 and 12 wk. TERT did not affect expression of Cdk4, cyc A, cyc D1, cyc E, retinoblastoma, p21, or p27.

TERT expression and activity were sustained in transgenic mice at 2–12 wk, with no decrease between the hyperplastic and hypertrophic stages (Fig. 3*D*).

TERT Triggers Hypertrophic Growth in Cultured Cardiac Myocytes. Because cardiac hypertrophy required active TERT but could not be explained by a described function of the protein, we also tested whether TERT might acutely induce hypertrophy in a postmitotic background, using viral gene transfer to neonatal rat ventricular myocytes. Under the conditions used, these are already refractory to G_1 exit in response to mitogenic serum (3). Telomerase activity was increased by wild-type TERT but not D868A TERT (Fig. 4*A*). TERT did not trigger DNA synthesis (Fig. 4*B Top*), but did cause myocyte enlargement (Fig. 4*B Middle* and *Bottom*), in agreement with the hypertrophic effect *in vivo*. Hypertrophy was produced by two independent TERT viruses, with and without green fluorescent protein to mark infected cells.

TERT Activates Molecular Markers and Mediators of Cardiac Hypertrophy. As with other triggers of hypertrophy (27, 34), the TERT transgene provoked ANF and βMHC expression in the heart (Fig. 4*C*). Although c-myc can regulate cell size and results from TERT in some cell types (35), no increase occurred in TERT transgenic mice, at either 2 or 12 wk (Fig. 4*D*), which concurs with the lack of Myc induction by TERT in a recent gain of function study (36). TERT also induced ANF acutely in culture (Fig. 4*E*).

Among potential mediators of hypertrophic growth, marked phosphorylation was seen for p70 S6K (37, 38), a pivotal

Table 1. TERT induces DNA synthesis and mitotic phosphorylation of histone H3 in postnatal ventricular myocytes

	BrdUrd (+) myocytes per 10^6			Phospho-H3 (+) myocytes per 10^6		
Age, wk	Control	αMHC-TERT	αMHC-D868A	Control	αMHC-TERT	αMHC-D868A
2	0	3,711	0	0	2,752	0
4	0	1,543	0	0	1,000	0
12	0	0	0	0	0	0

Transgenic mice and their littermates were analyzed by epifluorescence microscopy, using Abs against BrdUrd or the histone H3 Ser-10 phosphopeptide, plus Ab to sarcomeric MHC, a marker of myocyte identity. No change from the controls was seen in liver or small intestine (not shown).

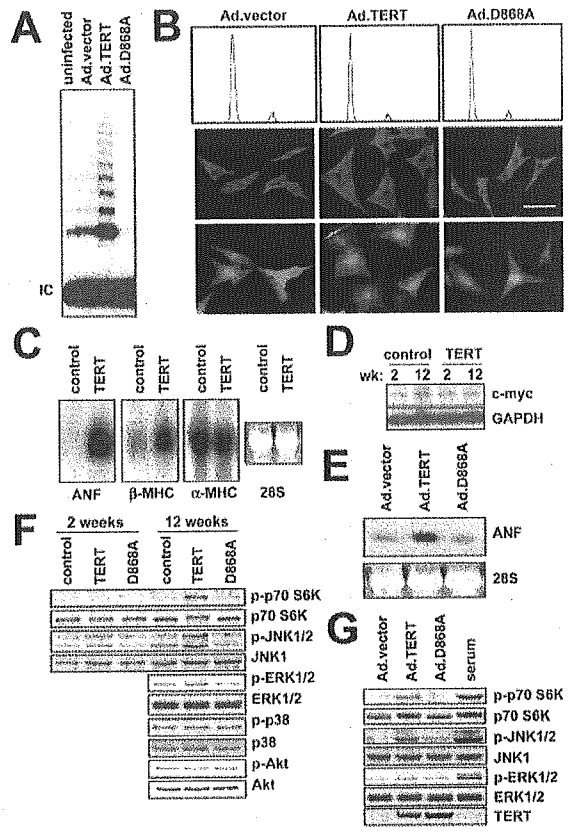

Fig. 4. Phosphorylation of p70 S6K and JNK during TERT-induced hypertrophy *in vivo* and *in vitro*. (*A*) Telomerase activity in rat ventricular myocytes after viral gene transfer, measured by the TRAP assay. IC, internal control template. (*B*) TERT elicits cardiac hypertrophy, not G_1 exit, in cultured ventricular myocytes. (*Top*) DNA histograms after viral gene transfer, using FITC-MF20 plus propidium iodide (PI) for flow cytometry. Cells were visualized with MF20 Ab to sarcomeric MHC (red; *Middle*) or coexpressed green fluorescent protein (green; *Bottom*). [Bar = 20 μm.] (*C*) Northern blot analysis of myocardium, showing induction of ANF and βMHC by the TERT transgene. (*D*) Northern blot analysis of myocardium, showing no change in c-myc expression by TERT. (*E*) Northern blot analysis of cultured cardiac myocytes, showing induction of ANF by viral delivery of TERT. (*F* and *G*) Western blot analysis showing phosphorylation of p70 S6K and JNK in myocardium of TERT transgenic mice (*F*) and in myocytes 24 h after viral delivery of TERT (*G*). In *G*, cardiac myocytes were treated with serum for 30 min as a positive control. Blots were reprobed for TERT to confirm equal expression of the wild-type and mutant proteins.

regulator of translation, at T389, the rapamycin-sensitive residue (ref. 39; Fig. 4*F*). Akt activation was not increased, implicating an alternative p70 S6K kinase or decreased signaling by a p70 S6K phosphatase. Smaller but consistent increases were seen in activation of JNK and ERK, but not p38. Phosphorylation of p70 S6K and JNK also was increased by viral delivery of TERT (Fig. 4*G*). Inactive TERT had no effect.

TERT Alleviates Cardiac Apoptosis. Although mechanisms coupling telomeric signals to cell survival are only beginning to be understood (10), we tested whether exogenous TERT might have salutary effects for cardiac muscle. In cell culture, nucleosomal DNA fragmentation at 24 h and cell death by 48 h were induced by serum-free insulin-free medium (Fig. 5 *A* and *B*). Protection was conferred by TERT, measured by both parameters, and required the active protein. Based on this cell culture result, we

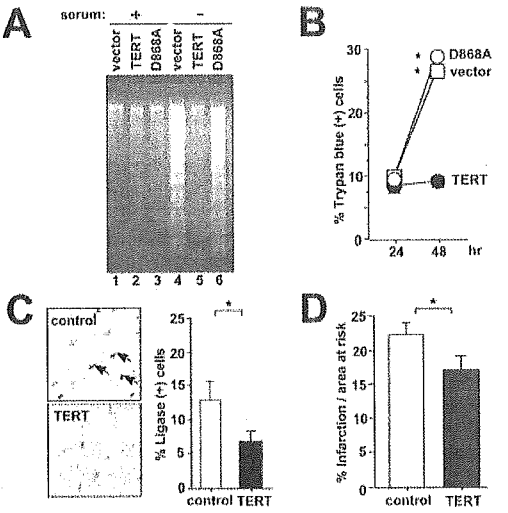

Fig. 5. TERT inhibits cardiac myocyte apoptosis *in vitro* and *in vivo*. (*A*) Nucleosomal DNA fragmentation. Cardiac myocytes were infected for 6 h then cultured for 18 h. DNA fragmentation induced by serum-free insulin-free medium was blocked by active TERT. (*B*) Cardiac myocyte survival. Cardiac myocytes were infected as shown, cultured in serum-free insulin-free medium for the indicated times, and analyzed by trypan blue exclusion. (*C Left*) Myocardium analyzed by the *in situ* ligase method 6 h after coronary artery occlusion. The arrows indicate Apoptotic nuclei (brown); sections were counterstained with nuclear fast red. (*Right*) Prevalence of myocyte apoptosis 6 h after coronary occlusion. *, $P < 0.01$; $n \geq 7$. (*D*) Infarct size in wild-type and TERT transgenic mice 24 h after coronary occlusion, expressed as a percentage of the area at risk. *, $P < 0.05$; $n \geq 6$.

then tested the prediction that TERT might protect against cardiac myocyte apoptosis *in vivo*, after ischemic injury (28). The prevalence of apoptosis after coronary ligation was reduced 50% by TERT (Fig. 5*C*), and the subsequent area of infarction was reduced by 23% (Fig. 5*D*). Similar results were seen in all four TERT transgenic lines.

Discussion

Mechanisms that impose a postmitotic phenotype in cardiac myocytes include decreased expression or function of essential cell cycle mediators and increased expression of cell cycle inhibitors (1). Progress toward cardiac myocyte regeneration has been slow, perhaps because of confounding redundancies among the cyclins, Cdks, Cdk inhibitors, pocket proteins, and E2F transcription factors. An alternative explanation may be a requirement for factors outside these alone, and telomerase activity thus has become an important focus of research on cell senescence and immortalization (5–10, 14). Our investigations establish that forcible expression of TERT, by itself, can prevent the loss of telomerase activity in postmitotic myocardium, maintain telomere length, and delay cardiac cell cycle exit. Prolongation of Cdk2 and Cdk6 activity, yet not Cdk4, conforms to its respective role in terminal differentiation by erythroid cells (40). By 3 months of age, however, Cdk activity and proliferation subsided despite equivalent telomerase activity. This result suggests the lack of an impetus to G_1 exit in adult myocardium, or perhaps further inhibitory signals, and concurs with other evidence for proliferative signaling by TERT only under mitogenic conditions (36). Overcoming senescence can require not just TERT, but also inactivation of pocket proteins or loss of INK4 Cdk inhibitors (12, 41). It will be intriguing to test whether such synergy exists in postmitotic cardiac muscle and whether endogenous TERT is induced by genes that promote cardiac

hyperplasia, like Myc (33), which activates TERT transcription directly (7).

Less expected was the later hypertrophy induced by TERT, also produced by viral delivery in cultured cardiac myocytes. A feature common to both settings was phosphorylation of p70 S6K at the key rapamycin-sensitive residue. p70 S6K controls the translation of mRNAs containing a 5′ oligopyrimidine tract, and the predominant effect of S6K in *Drosophila* is on cell size not cell number (39). In cardiac myocytes, p70 S6K is activated during diverse forms of hypertrophy (37, 38): inhibition by rapamycin underscores its essential function in hypertrophic growth but also that transcriptional "reprogramming" in hypertrophy occurs by an independent means (37). The concurrent activation of JNK by TERT, *in vitro* and *in vivo*, suggests one explanation for this observation (29). We have not detected reactivation of endogenous TERT in several mouse models of hypertrophy (not shown), but these do not emulate the increase in ploidy found in human heart failure.

In summary, preventing the down-regulation of TERT delays the timing of cardiac cell cycle exit and the postmitotic phenotype. Subsequent hypertrophy elicited by TERT was well tolerated, unlike many forms of induced cardiac growth (27, 34). Directly or indirectly, TERT also protected cardiac myocytes from apoptosis, consistent with evidence that telomerase or associated proteins promote cell survival (15, 16) at least in some settings (35). Relief of growth arrest could be independent of relief from apoptosis or might be linked, e.g., by components of a DNA damage-checkpoint pathway (10). For mice, where telomere length is much greater than for humans, alternatives to telomere length *per se* are attractive to explain effects of TERT on cell growth and survival, such as acting via telomere structure instead. A second, potentially related possibility would be the existence in mammals of telomeric silencing, as in yeast (7).

We thank Calvin Harley (Geron, Menlo Park, CA) and Jeffrey Robbins (Univ. of Cincinnati) for reagents, and Steve Elledge, Wade Harper, and Vicki Lundblad for suggestions. This work was supported in part by National Institutes of Health grants (to M.D.S.) and by the M. D. Anderson Foundation Professorship.

1. MacLellan, W. R. & Schneider, M. D. (2000) *Annu. Rev. Physiol.* **62,** 289–320.
2. Lipinski, M. M. & Jacks, T. (1999) *Oncogene* **18,** 7873–7882.
3. Akli, S., Zhan, S., Abdellatif, M. & Schneider, M. D. (1999) *Circ. Res.* **85,** 319–328.
4. Soonpaa, M. H., Koh, G. Y., Pajak, L., Jing, S. L., Wang, H., Franklin, M. T., Kim, K. K. & Field, L. J. (1997) *J. Clin. Invest.* **99,** 2644–2654.
5. Bodnar, A. G., Ouellette, M., Frolkis, M., Holt, S. E., Chiu, C. P., Morin, G. B., Harley, C. B., Shay, J. W., Lichtsteiner, S. & Wright, W. E. (1998) *Science* **279,** 349–352.
6. Hahn, W. C., Counter, C. M., Lundberg, A. S., Beijersbergen, R. L., Brooks, M. W. & Weinberg, R. A. (1999) *Nature (London)* **400,** 464–468.
7. McEachern, M. J., Krauskopf, A. & Blackburn, E. H. (2000) *Annu. Rev. Genet.* **34,** 331–358.
8. Shay, J. W. & Wright, W. E. (2001) *Science* **291,** 839–840.
9. Griffith, J. D., Comeau, L., Rosenfield, S., Stansel, R. M., Bianchi, A., Moss, H. & de Lange, T. (1999) *Cell* **97,** 503–514.
10. Karlseder, J., Broccoli, D., Dai, Y., Hardy, S. & de Lange, T. (1999) *Science* **283,** 1321–1325.
11. Prowse, K. R. & Greider, C. W. (1995) *Proc. Natl. Acad. Sci. USA* **92,** 4818–4822.
12. Dickson, M. A., Hahn, W. C., Ino, Y., Ronfard, V., Wu, J. Y., Weinberg, R. A., Louis, D. N., Li, F. P. & Rheinwald, J. G. (2000) *Mol. Cell. Biol.* **20,** 1436–1447.
13. Liu, Y., Snow, B. E., Hande, M. P., Yeung, D., Erdmann, N. J., Wakeham, A., Itie, A., Siderovski, D. P., Lansdorp, P. M., Robinson, M. O. & Harrington, L. (2000) *Curr. Biol.* **10,** 1459–1462.
14. Artandi, S. E. & DePinho, R. A. (2000) *Nat. Med.* **6,** 852–855.
15. Goytisolo, F. A., Samper, E., Martin-Caballero, J., Finnon, P., Herrera, E., Flores, J. M., Bouffler, S. D. & Blasco, M. A. (2000) *J. Exp. Med.* **192,** 1625–1636.
16. Herbert, B., Pitts, A. E., Baker, S. I., Hamilton, S. E., Wright, W. E., Shay, J. W. & Corey, D. R. (1999) *Proc. Natl. Acad. Sci. USA* **96,** 14276–14281.
17. Borges, A. & Liew, C. C. (1997) *J. Mol. Cell. Cardiol.* **29,** 2717–2724.
18. Yamaguchi, Y., Nozawa, K., Savoysky, E., Hayakawa, N., Nimura, Y. & Yoshida, S. (1998) *Exp. Cell Res.* **242,** 120–127.
19. Martin-Rivera, L., Herrera, E., Albar, J. P. & Blasco, M. A. (1998) *Proc. Natl. Acad. Sci. USA* **95,** 10471–10476.
20. Gidh-Jain, M., Huang, B. Y., Jain, P., Gick, G. & El-Sherif, N. (1998) *J. Mol. Cell. Cardiol.* **30,** 627–637.
21. Kiaris, H. & Schally, A. V. (1999) *Proc. Natl. Acad. Sci. USA* **96,** 226–231.
22. Kim, N. W. & Wu, F. (1997) *Nucleic Acids Res.* **25,** 2595–2597.
23. Broccoli, D., Godley, L. A., Donehower, L. A., Varmus, H. E. & de Lange, T. (1996) *Mol. Cell. Biol.* **16,** 3765–3772.
24. Counter, C. M., Avilion, A. A., LeFeuvre, C. E., Stewart, N. G., Greider, C. W., Harley, C. B. & Bacchetti, S. (1992) *EMBO J.* **11,** 1921–1929.
25. Weinrich, S. L., Pruzan, R., Ma, L., Ouellette, M., Tesmer, V. M., Holt, S. E., Bodnar, A. G., Lichtsteiner, S., Kim, N. W., Trager, J. B., *et al.* (1997) *Nat. Genet.* **17,** 498–502.
26. Subramaniam, A., Jones, W. K., Gulick, J., Wert, S., Neumann, J. & Robbins, J. (1991) *J. Biol. Chem.* **266,** 24613–24620.
27. Zhang, D., Gaussin, V., Taffet, G. E., Belaguli, N. S., Yamada, M., Schwartz, R. J., Michael, L. H., Overbeek, P. A. & Schneider, M. D. (2000) *Nat. Med.* **6,** 556–563.
28. Kurrelmeyer, K. M., Michael, L. H., Baumgarten, G., Taffet, G. E., Peschon, J. J., Sivasubramanian, N., Entman, M. L. & Mann, D. L. (2000) *Proc. Natl. Acad. Sci. USA* **97,** 5456–5461. (First Published April 25, 2000; 10.1073/pnas.070036297)
29. Choukroun, G., Hajjar, R., Fry, S., del Monte, F., Haq, S., Guerrero, J. L., Picard, M., Rosenzweig, A. & Force, T. (1999) *J. Clin. Invest.* **104,** 391–398.
30. Wei, Y., Mizzen, C. A., Cook, R. G., Gorovsky, M. A. & Allis, C. D. (1998) *Proc. Natl. Acad. Sci. USA* **95,** 7480–7484.
31. Negoro, S., Oh, H., Tone, E., Kunisada, K., Fujio, Y., Walsh, K., Kishimoto, T. & Yamauchi-Takihara, K. (2001) *Circulation* **103,** 555–561.
32. Didenko, V. V. & Hornsby, P. J. (1996) *J. Cell Biol.* **135,** 1369–1376.
33. Jackson, T., Allard, M. F., Sreenan, C. M., Doss, L. K., Bishop, S. P. & Swain, J. L. (1990) *Mol. Cell. Biol.* **10,** 3709–3716.
34. Molkentin, J. D., Lu, J. R., Antos, C. L., Markham, B., Richardson, J., Robbins, J., Grant, S. R. & Olson, E. N. (1998) *Cell* **93,** 215–228.
35. Wang, J., Hannon, G. J. & Beach, D. H. (2000) *Nature (London)* **405,** 755–756.
36. González-Suárez, E., Samper, E., Ramírez, A., Flores, J. M., Martín-Caballero, J., Jorcano, J. L. & Blasco, M. A. (2001) *EMBO J.* **20,** 2619–2630.
37. Sadoshima, J. & Izumo, S. (1995) *Circ. Res.* **77,** 1040–1052.
38. Oh, H., Fujio, Y., Kunisada, K., Hirota, H., Matsui, H., Kishimoto, T. & Yamauchi-Takihara, K. (1998) *J. Biol. Chem.* **273,** 9703–9710.
39. Volarevic, S. & Thomas, G. (2000) *Prog. Nucleic Acid Res. Mol. Biol.* **65,** 101–127.
40. Matushansky, I., Radparvar, F. & Skoultchi, A. I. (2000) *Proc. Natl. Acad. Sci. USA* **97,** 14317–14322. (First Published December 12, 2000; 10.1073/pnas.250488697)
41. Kiyono, T., Foster, S. A., Koop, J. I., McDougall, J. K., Galloway, D. A. & Klingelhutz, A. J. (1998) *Nature (London)* **396,** 84–88.

Telomere attrition and Chk2 activation in human heart failure

Hidemasa Oh*†, Sam C. Wang*†, Arun Prahash*†, Motoaki Sano*†, Christine S. Moravec‡, George E. Taffet†§, Lloyd H. Michael†§, Keith A. Youker†§, Mark L. Entman†§, and Michael D. Schneider*†¶‖**

*Center for Cardiovascular Development, §Methodist Hospital DeBakey Heart Center, and Departments of †Medicine, ¶Molecular and Cellular Biology, and ‖Molecular Physiology and Biophysics, Baylor College of Medicine, Houston, TX 77030; and ‡Department of Cardiovascular Medicine, Cleveland Clinic Foundation, Cleveland, OH 44195

Edited by Robert A. Weinberg, Whitehead Institute for Biomedical Research, Cambridge, MA, and approved March 3, 2003 (received for review October 2, 2002)

The "postmitotic" phenotype in adult cardiac muscle exhibits similarities to replicative senescence more generally and constitutes a barrier to effective restorative growth in heart disease. Telomere dysfunction is implicated in senescence and apoptotic signaling but its potential role in heart disorders is unknown. Here, we report that cardiac apoptosis in human heart failure is associated specifically with defective expression of the telomere repeat-binding factor TRF2, telomere shortening, and activation of the DNA damage checkpoint kinase, Chk2. In cultured cardiomyocytes, interference with either TRF2 function or expression triggered telomere erosion and apoptosis, indicating that cell death can occur via this pathway even in postmitotic, noncycling cells; conversely, exogenous TRF2 conferred protection from oxidative stress. *In vivo*, mechanical stress was sufficient to down-regulate TRF2, shorten telomeres, and activate Chk2 in mouse myocardium, and transgenic expression of telomerase reverse transcriptase conferred protection from all three responses. Together, these data suggest that apoptosis in chronic heart failure is mediated in part by telomere dysfunction and suggest an essential role for TRF2 even in postmitotic cells.

The emerging concept of heart failure as a myocyte-deficiency disease is predicated on the limited regenerative capacity of mammalian cardiac muscle, which is inadequate to maintain pump function after cell death (1–4). Conceptually, approaches to augment cardiac myocyte number include cell grafting (5), driving nonmuscle cells to a cardiac "fate" (6), potentiating repair by endogenous stem cells (7), and alleviating apoptosis (8). A rational approach to such interventions encompasses identifying endogenous molecules that contribute to cell survival in the heart (9–12).

Telomere maintenance is one mechanism through which cell viability is preserved (13–21). Telomeres consist of tandem T2AG3 repeats at chromosome ends, maintained by telomerase reverse transcriptase (TERT), and bound by specific telomere repeat-binding factors (TRFs) including TRF1 and TRF2 (17, 20, 22, 23). We have shown that TERT and telomerase activity are down-regulated in adult mouse myocardium [unlike some other adult tissues in the mouse (24)], and that forced expression of TERT in transgenic mice can delay the timing of the cell cycle exit of cardiac myocytes (3). At later ages, continued expression of TERT at the level found in embryonic hearts had two other effects with possible therapeutic significance. First, TERT induced myocyte enlargement (hypertrophic growth), after the cessation of cycling. Second, TERT suppressed cardiac myocyte apoptosis both *in vitro* (serum starvation) and *in vivo* (ischemia-reperfusion injury).

In end-stage human heart failure, myocyte apoptosis increases typically to an incidence of 0.5–1% (25) but surprisingly little is known of the instigating or signal transducing events for cell death in this remarkably common disorder. We demonstrate here that failing human hearts have telomeres that are 25% shorter on average than age-matched controls, with decreased expression of TRF2 and marked activation of the DNA damage kinase, checkpoint kinase 2 (Chk2). Suppressing TRF2 function in cultured cardiac myocytes provoked telomere erosion, Chk2 kinase activation, and apoptosis, and an antisense "knockdown" of TRF2 did the same. Conversely, exogenous TRF2 conferred protection from oxidative stress. In mouse myocardium, biomechanical stress (partial aortic constriction) reduced telomere length within 1 week, provoked the loss of TRF2, and triggered Chk2 activation, all as seen in failing human hearts. Forced expression of telomerase prevented telomere erosion, down-regulation of TRF2, activation of Chk2, and myocyte apoptosis. Together, the results suggest a role for telomere dysfunction in heart failure via stress-induced down-regulation of TRF2.

Materials and Methods

Patient Samples and Controls. Human myocardium was obtained through the Methodist DeBakey Heart Center and the Human Heart Tissue Transplant Core of the Cleveland Clinic. Tissue procurement was based on patient-informed consents and approved by the respective institutional review boards. Heart failure tissue (idiopathic and ischemic dilated cardiomyopathy) was obtained from explanted hearts at the time of therapeutic transplantation. Normal hearts were obtained from unmatched organ donors and victims of motor vehicle accidents. Hypertrophic obstructive cardiomyopathy (HOCM), a heterogenous primary disorder of heart growth without ventricular pump failure, was also used for comparison.

Cell Culture and Viral Gene Transfer. Ventricular myocytes from 2-d-old Sprague–Dawley rats were purified and cultured (3, 26). By this age, ventricular myocytes become refractory to serum-induced G1 exit, after initial serum starvation *in vitro* (26). Plasmids for human TRF1, TRF2, and the corresponding dominant-negative truncations (TRF1$^{\Delta M}$ and TRF2$^{\Delta B\Delta M}$) were provided by T. de Lange (The Rockefeller University, New York; ref. 17). Adenoviruses coexpressing enhanced GFP were generated by using pAdTrack-cytomegalovirus and pShuttle-cytomegalovirus (provided by B. Volgelstein, Johns Hopkins Oncology Center, Baltimore; refs. 3 and 27). Myocytes were infected at a multiplicity of infection of 20. To visualize TRF1/2 after gene transfer, myocytes were fixed in 70% ethanol then incubated sequentially with tetramethyl rhodamine isothiocyanate-conjugated MF-20 Ab to sarcomeric myosin-heavy chains (MHCs) to confirm cell type (University of Iowa Hybridoma Bank, Iowa City), rabbit Abs to TRF1 and TRF2 (1:500; nos. 581420 and 581425, Calbiochem), and FITC-conjugated goat Ab to rabbit IgG (1:1,000, Sigma). Nuclei were stained with 4′,6-

This paper was submitted directly (Track II) to the PNAS office.

Abbreviations: MHC, myosin heavy chain; Chk2, checkpoint kinase 2; HOCM, hypertrophic obstructive cardiomyopathy; PARP, poly (ADP-ribose) polymerase; TERT, telomerase reverse transcriptase; TRF, telomere repeat-binding factor.

**To whom correspondence should be addressed. E-mail: michaels@bcm.tmc.edu.

www.pnas.org/cgi/doi/10.1073/pnas.0836098100

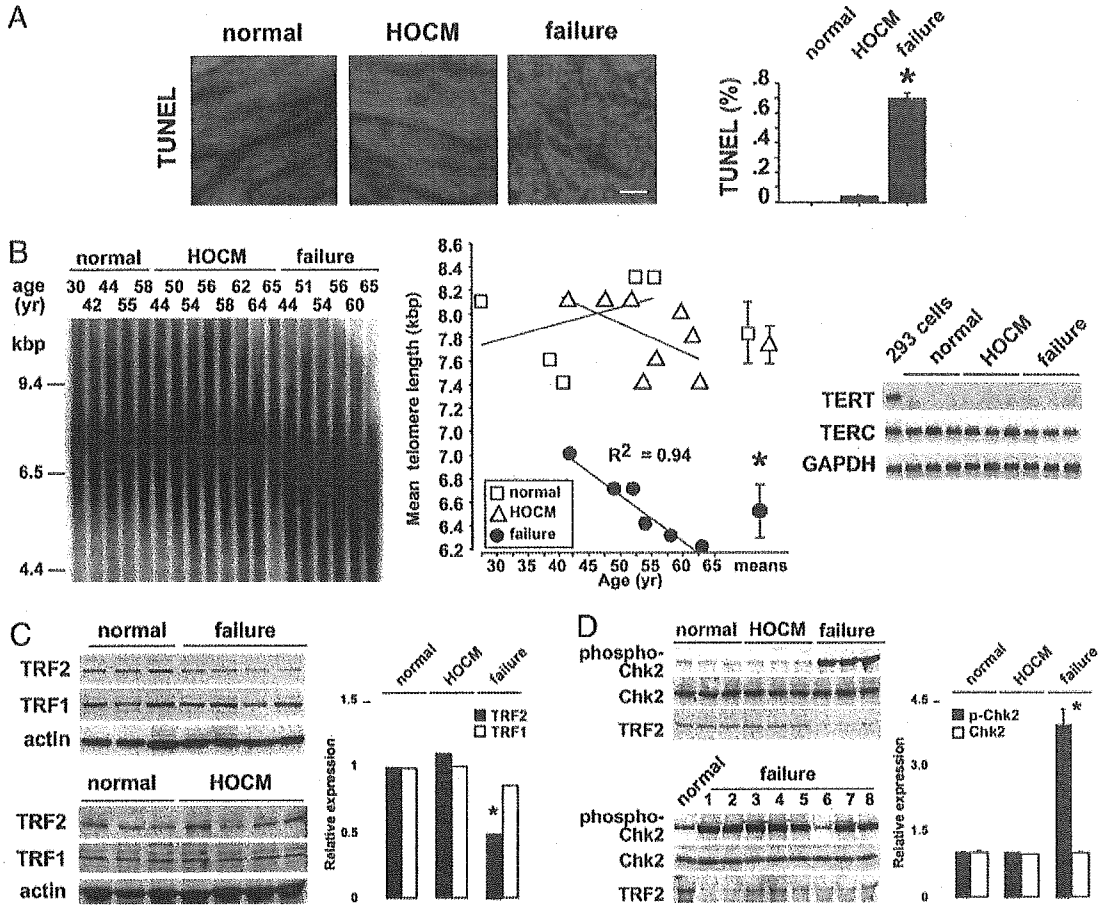

Fig. 1. Telomere dysfunction in human heart failure. (*A*) Cardiomyocyte apoptosis, shown by terminal transferase-mediated dUTP-biotin nick end-labeling and sarcomeric MHC staining, was comparable to the incidence in recent reports (25). *, $P = 0.0001$. (Bar = 10 μm.) (*B*) Cardiac telomere erosion. (*Left*) Southern blot using a telomere-specific probe. (*Center*) Telomere length as a function of age. *, $P = 0.0001$. (*Right*) Telomere erosion occurred without overt change in cardiac TERT or RNA component of telomerase (TERC) mRNA levels. (*C*) Loss of cardiac TRF2 protein in heart failure, shown by Western blot. *, $P = 0.0001$. (*D*) Activation of Chk2 (Thr-68 phosphorylation) in heart failure. *, $P = 0.002$. (*Lower*) Patient no. 6 illustrates the one counterexample without Chk2 activation despite decreased TRF2.

diamidino-2-phenylindole (DAPI). Images were captured with a Zeiss Axioplan 2 epifluorescence microscope.

Antisense Oligonucleotides. Three antisense phosphorothioate oligonucleotides for mouse TRF2 were generated (Molecula Research Laboratories, Herndon, VA), one of which inhibited endogenous TRF2 expression effectively in NIH 3T3 cells (data not shown). The sequences used were antisense TRF2 (asTRF2), 5′-CCTGGGCTGCCGGCTCGAGC-3′; sense TRF2 (sTRF2), 5′-CGAGCTCGGCCGTCGGGTCC-3′; and antisense GFP (28), 5′-CGTTTACGTCGCCGTCCAGC-3′. Oligonucleotides were transfected into 1- to 2-d-old C57BL/6 mouse cardiomyocytes, cultured as above, with Oligofectamine (Invitrogen).

Animal Models. Cardiac-specific TERT transgenic mice (*αMHC-TERT*; ref. 3) and wild-type littermates (10–12 weeks old and 18–22 g) were subjected for 1 week to partial occlusion of the transverse aorta (2). The control "sham" operation comprised anesthesia, thoracotomy, and ligature placement without constriction. The presence and severity of obstruction were corroborated by Doppler flow studies; only mice in which severe load was confirmed (a right to left carotid artery velocity ratio >3.5) were analyzed further. Doppler echocardiography and staining with Sirius red were performed 7 d after surgery (3).

Apoptosis. For myocardium, terminal transferase-mediated dUTP-biotin nick end-labeling assays were performed with the Oncor ApopTaq Direct *In Situ* Apoptosis Detection kit (2), MF20 Ab to sarcomeric MHC, and Texas red-conjugated Ab to mouse IgG. For cultured cardiomyocytes, hypodiploid DNA was detected with two-color flow cytometry by using propidium iodide for DNA content and FITC-conjugated MF20 (3, 26).

Telomere Length. DNA was digested with *Rsa*I, resolved by electrophoresis in 0.5% agarose, transferred to Hybond-N$^+$ membranes (Amersham Biosciences), and hybridized with a ^{32}P-labeled $(TTAGGG)_4$ telomeric probe (3, 29). Mean telomere length was ascertained by PhosphorImager scanning (Molecular Dynamics).

Telomerase Expression and Activity. Telomerase activity was measured by a PCR-based telomerase repeat amplification protocol assay and 1 μg of cell or tissue extract (3). TERT, the RNA component of telomerase, and GAPDH were analyzed by RT-PCR in the log-linear range of amplification (30–32).

Western Blot and Immune Complex Kinase Assays. Proteins were resolved by electrophoresis in 10% SDS-polyacrylamide gels and transferred to membranes by electroblotting. Abs were human

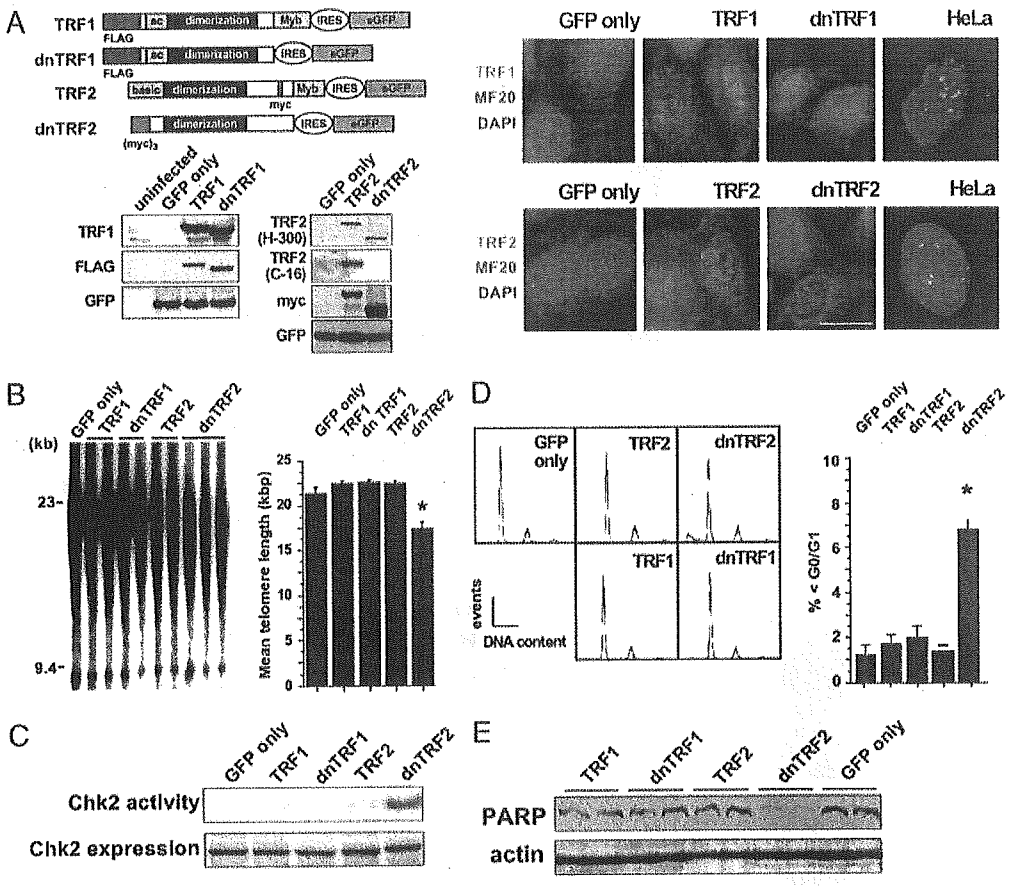

Fig. 2. Dominant-negative TRF2 triggers telomere dysfunction and apoptosis in cardiomyocytes. (*A*) Viral vectors. (*Upper Left*) TRF1 and TRF2 tagged with FLAG and myc epitopes, respectively (17). Dominant-negative TRF1 (TRF1$^{\Delta M}$) lacks the Myb telomere-binding domain; dominant-negative TRF2 (TRF2$^{\Delta B\Delta M}$) lacks the Myb domain and N-terminal basic domain (17). (*Lower Left*) Western blots confirming expression of the exogenous proteins in cardiomyocytes. dnTRF2 is detected with Ab H-300 (against amino acids 49–300) but not Ab C-16 (against the C terminus). (*Right*) Immunocytochemistry for the exogenous proteins in cardiomyocytes. TRF1/2, FITC; MF20, tetramethyl rhodamine isothiocyanate; nuclei, 4′,6-diamidino-2-phenylindole (DAPI). (Bar = 5 μm.) (*B*) Telomere shortening, shown by Southern blot. *, $P = 0.002$. (*C*) Activation of Chk2, shown by immune complex kinase assays. (*D*) Apoptosis, shown as hypodiploid DNA by flow cytometry. $n = 7$; *, $P = 0.0001$. (*E*) PARP cleavage, shown by Western blotting.

and mouse TRF2 (Calbiochem), human and mouse TRF1 (Calbiochem), phospho-Chk2 (Thr-68; Cell Signaling Technology, Beverly, MA), sarcomeric α-actin and myc (Sigma), FLAG epitope (M2, Kodak), GFP (CLONTECH), Chk2 (Santa Cruz Biotechnology), and poly (ADP-ribose) polymerase (PARP, Oncogene). To detect exogenous TRF2 in virus-infected cardiomyocytes, goat and rabbit Abs to TRF2 were used (C-16, H-300; Santa Cruz Biotechnology), and endogenous rat TRF2 was detected by using rabbit Ab to TRF2 (Alpha Diagnostic International, San Antonio, TX). After blocking with 5% nonfat milk plus 0.1% Tween 20, blots were incubated with primary Abs (1:500), horseradish peroxidase-conjugated secondary Abs (1:3,000; Amersham Biosciences), and enhanced chemiluminescence reagents (Amersham Biosciences).

To assay Chk2 activity, samples were lysed in 20 mM Tris·HCl (pH 8.0), 0.1% Triton X-100, 10 mM NaF, 1 mM $NaVa_3VO_4$, 10 μg/ml of aprotinin, and 1 mM PMSF and then incubated for 1 h with Ab to Chk2 and protein A/G-Sepharose (Amersham Biosciences). Immunoprecipitates were washed and assayed in the presence of 30 μM CHKtide substrate peptide (KKKVSRSGLYRSPSMPENLNRPR; Upstate Biotechnology, Lake Placid, NY), 40 μM adenosine triphosphate, and 15 μCi [γ-^{32}P]ATP for 30 min at 30°C (1 Ci = 37 GBq). Proteins were resolved by electrophoresis in SDS-polyacrylamide gels and visualized by autoradiography. Aliquots of Chk2 immunoprecipitates were also used for Western blotting, allowing activity and content to be compared in the same samples.

Statistical Analysis. Data, reported as the mean ± SE, were analyzed by ANOVA and Scheffé's test using a significance level of $P \leq 0.05$.

Results

Telomere Attrition, Loss of TRF2, and Checkpoint Kinase Activation in Human Heart Failure. To address the expression and function of telomeric proteins in human heart disease, we analyzed cardiac muscle from patients with end-stage heart failure at the time of transplantation, HOCM undergoing therapeutic partial resection of the septum, and normal myocardium. The prevalence of apoptosis (Fig. 1*A*) increased markedly in heart failure (0.70 ± 0.04% by terminal transferase-mediated dUTP-biotin nick end-labeling assay; normal <0.005%, $P = 0.0001$; HOCM 0.04 ± 0.001%, $P = 0.0001$; $n = 8$ for each group), comparable to recent reports (25). We next examined telomere length, telomerase activity, and TRF1/2 expression using heart samples well matched for age and sex. Mean telomere length (Fig. 1*B Left*) was reduced 25% in failing hearts (6.5 ± 0.2 kb), compared with normal samples (7.8 ± 0.2 kb, $P = 0.0001$) or patients with

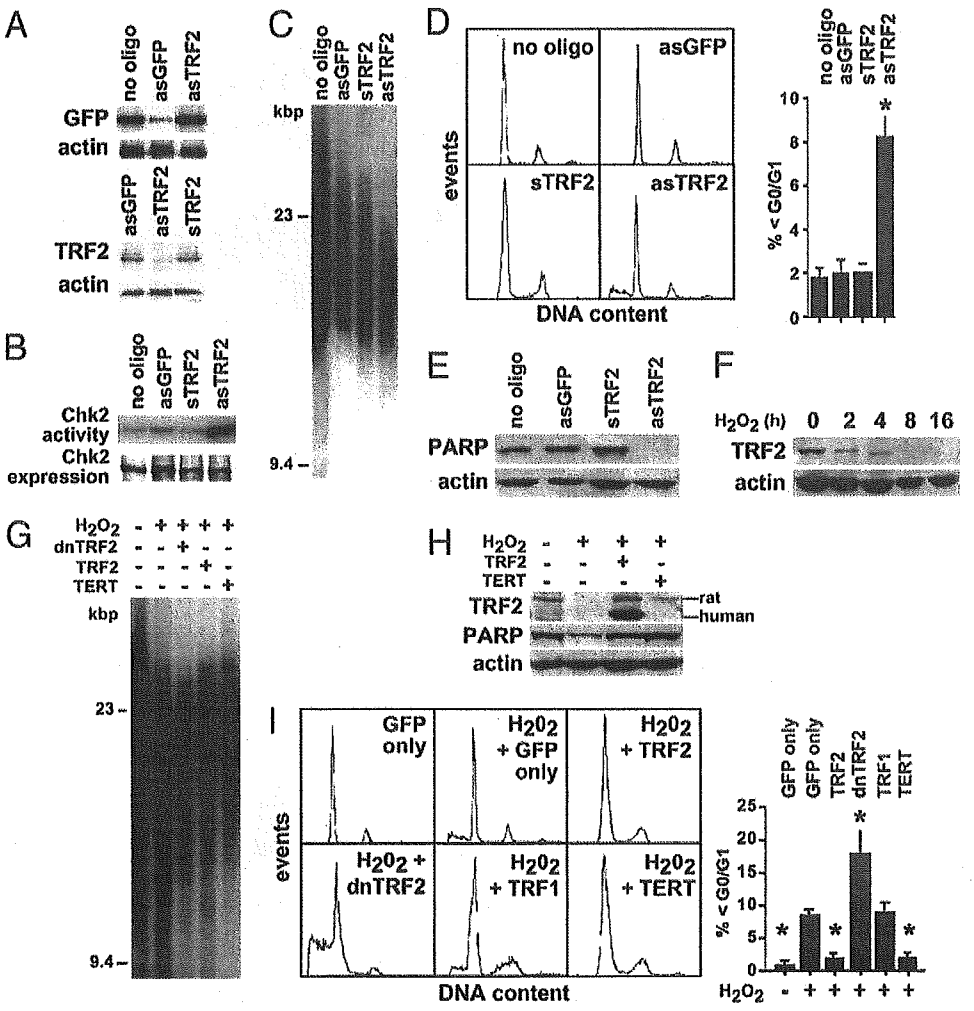

Fig. 3. Down-regulation of endogenous TRF2 in cardiomyocytes by antisense (as) oligonucleotide or oxidative stress. (*A–E*) Mouse cardiomyocytes were transfected as indicated for 48 h. (*A*) Reduction of TRF2 specifically by asTRF2 (Western blot). Adenoviral delivery of GFP was used for all myocytes (*Upper*). (*B*) Chk2 activation (immune complex kinase assay). (*C*) Telomere shortening (Southern blot). (*D*) Cardiomyocyte apoptosis (flow cytometry). $n \geq 5$; $P = 0.0001$. (*E*) PARP cleavage (Western blot). (*F–I*) Rat cardiomyocytes infected with the viruses shown were treated 48 h later with 100 μM H_2O_2 for 8 h. (*F*) Western blot showing rapid down-regulation of TRF2 by H_2O_2. Telomere shortening (*G*), PARP cleavage (*H*), and apoptosis (*I*) were each induced by H_2O_2 and rescued by viral delivery of TRF2 or TERT. $n \geq 6$; $P < 0.02$.

HOCM (7.7 ± 0.1 kb, $P = 0.0001$). Although the RNA component of telomerase was present in all three groups without significant difference, neither telomerase activity nor TERT expression was detected, in any of the three groups, by using a telomeric repeat amplification protocol (data not shown) and RT-PCR for 30 cycles, respectively (Fig. 1*B Right*). The paucity of telomerase activity in adult human myocardium concurs with our prior findings in mice (3) and suggests a mechanism other than defective telomerase activity for the loss of telomere length in failing hearts.

To test one alternative mechanism for telomere dysfunction (17, 33), TRF1 and TRF2 were examined (Fig. 1*C*). Both proteins were readily detected in normal adult human myocardium, with no change in HOCM. By contrast, in patients with heart failure, TRF2 was down-regulated 50 ± 8% ($P = 0.0001$; range 25–75%). Interference with endogenous TRF2 activates apoptosis via the ataxia-telangiectasia mutated (ATM) protein kinase (17), and partial loss of TRF2 is the earliest event in some forms of telomere shortening (33). Consistent with this reported pathway, phosphorylation of Chk2 at Thr-68, the principal site for activation by ATM (34), was apparent in 12 of 14 failing hearts but in none of the normal controls or patients with HOCM (Fig. 1*D* and data not shown). Chk2 levels were unaffected.

Interference with Endogenous TRF2 Triggers Telomere Dysfunction and Apoptosis in Postmitotic Cardiomyocytes. To ascertain whether the inferred pathway from TRF2 to Chk2 is operative in postmitotic cardiomyocytes (which might differ from cycling cells), we expressed epitope-tagged dominant-negative and wild-type TRF2 and TRF1 in primary culture using adenoviral vectors (Fig. 2*A*). At the stage tested, cardiomyocytes are already growth-arrested *in vivo* and refractory to mitogenic serum (3, 26). All four constructs were expressed uniformly. Staining was most intense in the nuclei, with a heterogenous intranuclear distribution similar to that of endogenous TRF1/2 (Fig. 2*A*). Myc-tagged dominant-negative TRF2 induced telomere erosion (Fig. 2*B*), accompanied by Chk2 activation (Fig. 2*C*), PARP cleavage (indicative of caspase-3 activity; Fig. 2*E*), and apoptosis (Fig. 2*D*). Myc-tagged wild-type TRF2, FLAG-tagged wild-type TRF1, and FLAG-tagged dominant-negative TRF1 had no effect (Fig. 2 *B–E*).

Because dominant-negative mutations are not formally equivalent to reduced expression, we confirmed the above findings by using an antisense oligonucleotide for TRF2 vs. the sense strand TRF2 control and an irrelevant antisense oligonucleotide against GFP. In cardiomyocytes, TRF2 and GFP were specifically reduced by the respective antisense oligonucleotides (Fig. 3*A*). Reduction of endogenous TRF2 provoked the same responses as did the dominant inhibitor: telomere shortening, Chk2 activation, PARP cleavage, and apoptosis (Fig. 3 *B–E*). Thus, interference with TRF2 causes apoptosis and activation of Chk2 even in postmitotic, noncycling cells.

TRF2 and TERT Protect Cardiomyocytes from Pathophysiological Stress. Endogenous TRF2 in cardiomyocytes decreased within 2 h of oxidative stress (100 μM H_2O_2; Fig. 3*F*). Compared with a viral control expressing GFP alone, either TRF2 or TERT rescued the adverse effect of H_2O_2 on telomere length, PARP cleavage, and apoptosis (Fig. 3 *G–I*), consistent with earlier evidence for cardioprotection by TERT (3). Dominant-negative TRF2 markedly potentiated the effect of H_2O_2 on apoptosis (Fig. 3*I*) but not on telomere length (Fig. 3*G*); thus, telomere attrition does not simply reflect the extent of apoptosis.

Mechanical load activates signaling cascades including oxidative stress (35), predisposes cardiac muscle to late-onset apoptosis (36), and can trigger apoptosis acutely, especially in susceptible backgrounds (9, 11). To test whether mechanical load might induce telomere dysfunction in myocardium, adult mice were subjected to severe aortic constriction. By comparison to littermate controls undergoing the control procedure, telomere length was reduced 3 kbp by increased load for 7 d (n = 4; $P \leq 0.01$; Fig. 4*A*). Under the conditions tested, mechanical load also triggered down-regulation of TRF2 by 52 ± 2% ($P \leq$ 0.001; Fig. 4*B*), induced Chk2 kinase activity (P = 0.002; Fig. 4*C*), and induced apoptosis (0.32 ± 0.06%; P = 0.0003; Fig. 4*D*).

In culture, TERT largely prevented the loss of endogenous TRF2 provoked by oxidative stress (Fig. 3*H*). Forced expression of TERT in adult myocardium maintains telomere length and confers protection from apoptosis after ischemia-reperfusion injury (3). Hence, we tested whether TERT might attenuate or rescue telomere dysfunction induced by severe mechanical load. As reported previously (3), telomere length was 21.5 ± 0.5 kbp in the *αMHC-TERT* mice and 3 kbp longer than the length in wild-type littermates (n = 4; $P \leq 0.01$; Fig. 4*A*). By contrast to the sequelae of biomechanical stress in wild-type animals, *αMHC-TERT* mice were refractory to telomere erosion (Fig. 4*A*), loss of TRF2 (Fig. 4*B*), Chk2 kinase activation (Fig. 4*C*), and apoptosis (Fig. 4*D*). Consistent with the inhibition of cardiomyocyte death, *αMHC-TERT* mice had less replacement fibrosis after banding and better preservation of left ventricular ejection velocity, a measure of systolic function (Fig. 4*D*).

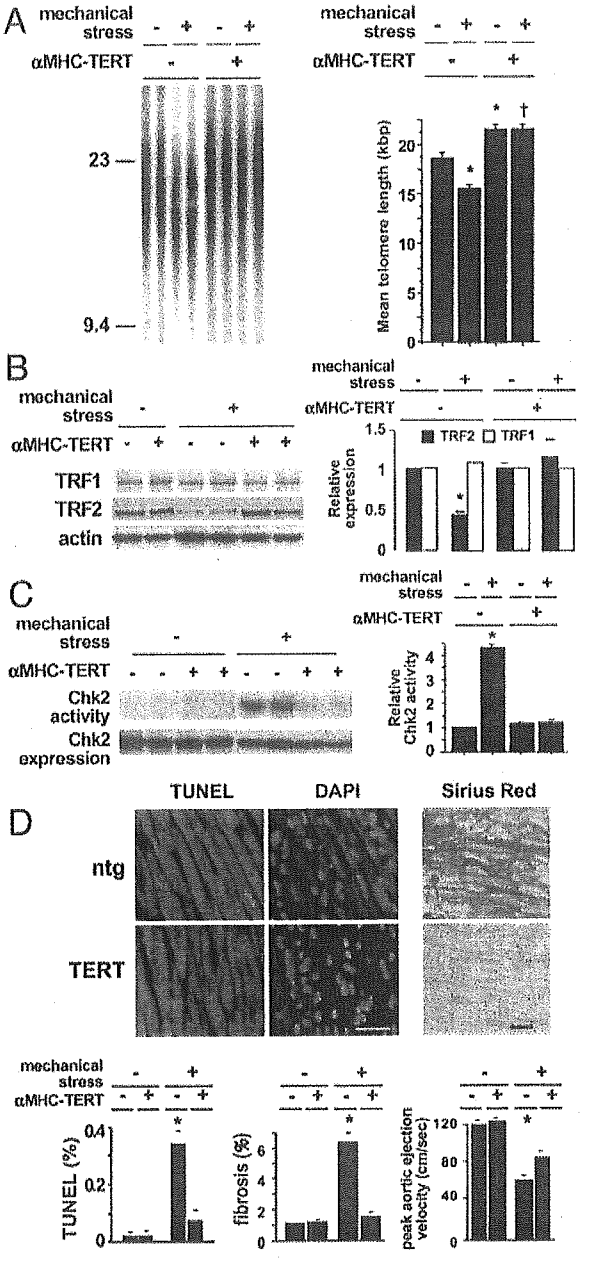

Fig. 4. TERT protects adult mouse myocardium from telomere shortening, apoptosis, fibrosis, and systolic dysfunction after biomechanical stress. *αMHC-TERT* mice and nontransgenic littermates (ntg) were analyzed 7 d after severe aortic constriction. Telomere length (*A*), TRF2 levels (*B*), and Chk2 kinase activation (*C*) were measured as in Fig. 2. *, $P \leq 0.01$ vs. ntg without banding; †, P = 0.0001 vs. ntg with banding. (*D Upper*) Representative terminal transferase-mediated dUTP-biotin nick end-labeling and Sirius red staining, in banded mice. (*D Lower*) Mean results ± SE are shown for apoptosis (*Left*), fibrosis (*Center*), and peak aortic ejection velocity by Doppler echocardiography (*Right*). *, P = 0.0001. (Bar = 20 μm.)

Discussion

In summary, telomere shortening and down-regulation of the telomere end-capping protein, TRF2, occur in end-stage human heart failure. Neither telomere erosion nor loss of TRF2 was observed in normal hearts at the ages tested, and neither occurred in hypertrophy if failure was absent. Thus, telomere dysfunction in myocardium is not, at least overtly, a feature of normal aging, as in proliferating cells, and is not a mere result of hypertrophic growth. The fraction of actively cycling myocytes in adult myocardium is minuscule at best (1, 4), and the prevalence of apoptosis in failing hearts was six to seven per thousand. Hence, the 25% loss of telomere length here can neither be explained by the "end-replication" problem nor by generalized DNA fragmentation (37). In cultured cardiac myocytes, interference with endogenous TRF2 triggered rapid telomere shortening, activation of Chk2, and apoptosis, without cell cycle reentry. Importantly, antisense reduction of endogenous TRF2 had comparable adverse effects, and exogenous TRF2 was protective against oxidative stress, at least in culture. In adult mouse myocardium, severe mechanical load for just 1 week down-regulated endogenous TRF2, shortened telomeres, and activated Chk2. Forced expression of TERT, at levels normal for the embryonic heart, rescued all three responses. Our results suggest the likelihood of active telomere erosion in human heart

failure, possibly contingent on the down-regulation of TRF2 in diseased myocardium, and implicate oxidative stress as one signal for this loss. Interestingly, telomere loss is likewise associated with heart failure in fifth-generation mice lacking the RNA component of telomerase (38).

Preservation of TRF2 levels and suppression of Chk2 activity by TERT, after mechanical stress, together provide further genetic evidence for the potential use of telomerase in cardiac protection and repair (3). Telomere structure, not length *per se*, is the prerequisite for normal telomere function (23), and a decrease in TRF2 is thought to be the rate-limiting step for some forms of apoptosis (33). TRF2 is essential to form the lariat-like loop at chromosome ends that protects the 3′ single-stranded overhang from degradation (23, 39). One pathway that might be expected to promote telomere shortening in this context is the unopposed action of TRF1 and TRF1-binding proteins. Also, TRF2 recruits a number of proteins to the telomere including Ku (the regulatory component of DNA-dependent protein kinase), Nijmegen breakage syndrome 1 (a component of the Mre11 DNA repair complex), and the Werner syndrome helicase, which all are required for telomere maintenance (40, 41). Predisposition to apoptosis is a known consequence of defects in each of these proteins, whose importance in heart failure is untested.

We thank the physicians of the Methodist Hospital DeBakey Heart Center, Cleveland Clinic Heart Transplant Teams, and Life Banc of Northeast Ohio; L. Shirley, J. Pocius, A. Aldape, and C. Scott for technical assistance; and V. Lundblad and S. Elledge for helpful suggestions. This work was supported by National Institutes of Health grants (to M.D.S., L.H.M., and M.L.E.), the Howard Hughes Medical Institute Research Training Fellowship for Medical Students (to S.C.W.), and the M. D. Anderson Foundation Professorship (to M.D.S.).

1. MacLellan, W. R. & Schneider, M. D. (2000) *Annu. Rev. Physiol.* **62,** 289–320.
2. Zhang, D., Gaussin, V., Taffet, G. E., Belaguli, N. S., Yamada, M., Schwartz, R. J., Michael, L. H., Overbeek, P. A. & Schneider, M. D. (2000) *Nat. Med.* **6,** 556–563.
3. Oh, H., Taffet, G. E., Youker, K. A., Entman, M. L., Overbeek, P. A., Michael, L. H. & Schneider, M. D. (2001) *Proc. Natl. Acad. Sci. USA* **98,** 10308–10313.
4. Pasumarthi, K. B. & Field, L. J. (2002) *Circ. Res.* **90,** 1044–1054.
5. Koh, G. Y., Soonpaa, M. H., Klug, M. G., Pride, H. P., Cooper, B. J., Zipes, D. P. & Field, L. J. (1995) *J. Clin. Invest.* **96,** 2034–2042.
6. Grepin, C., Nemer, G. & Nemer, M. (1997) *Development (Cambridge, U.K.)* **124,** 2387–2395.
7. Jackson, K. A., Majka, S. M., Wang, H., Pocius, J., Hartley, C. J., Majesky, M. W., Entman, M. L., Michael, L. H., Hirschi, K. K. & Goodell, M. A. (2001) *J. Clin. Invest.* **107,** 1395–1402.
8. Reed, J. C. & Paternostro, G. (1999) *Proc. Natl. Acad. Sci. USA* **96,** 7614–7616.
9. Hirota, H., Chen, J., Betz, U. A., Rajewsky, K., Gu, Y., Ross, J., Jr., Muller, W. & Chien, K. R. (1999) *Cell* **97,** 189–198.
10. Kubasiak, L. A., Hernandez, O. M., Bishopric, N. H. & Webster, K. A. (2002) *Proc. Natl. Acad. Sci. USA* **99,** 12825–12830.
11. Sadoshima, J., Montagne, O., Wang, Q., Yang, G., Warden, J., Liu, J., Takagi, G., Karoor, V., Hong, C., Johnson, G. L., *et al.* (2002) *J. Clin. Invest.* **110,** 271–279.
12. Yussman, M. G., Toyokawa, T., Odley, A., Lynch, R. A., Wu, G., Colbert, M. C., Aronow, B. J., Lorenz, J. N. & Dorn, G. W. (2002) *Nat. Med.* **8,** 725–730.
13. Lee, H. W., Blasco, M. A., Gottlieb, G. J., Horner, J. W., 2nd, Greider, C. W. & DePinho, R. A. (1998) *Nature* **392,** 569–574.
14. Hahn, W. C., Stewart, S. A., Brooks, M. W., York, S. G., Eaton, E., Kurachi, A., Beijersbergen, R. L., Knoll, J. H. M., Meyerson, M. & Weinberg, R. A. (1999) *Nat. Med.* **5,** 1164–1170.
15. Weinert, T. & Lundblad, V. (1999) *Nat. Genet.* **21,** 151–152.
16. Wong, K. K., Chang, S., Weiler, S. R., Ganesan, S., Chaudhuri, J., Zhu, C., Artandi, S. E., Rudolph, K. L., Gottlieb, G. J., Chin, L., *et al.* (2000) *Nat. Genet.* **26,** 85–88.
17. Karlseder, J., Broccoli, D., Dai, Y., Hardy, S. & de Lange, T. (1999) *Science* **283,** 1321–1325.
18. Hemann, M. T., Rudolph, K. L., Strong, M. A., DePinho, R. A., Chin, L. & Greider, C. W. (2001) *Mol. Biol. Cell* **12,** 2023–2030.
19. Stewart, S. A. & Weinberg, R. A. (2002) *Oncogene* **21,** 627–630.
20. de Lange, T. (2002) *Oncogene* **21,** 532–540.
21. Chang, S. & DePinho, R. A. (2002) *Proc. Natl. Acad. Sci. USA* **99,** 12520–12522.
22. McEachern, M. J., Krauskopf, A. & Blackburn, E. H. (2000) *Annu. Rev. Genet.* **34,** 331–358.
23. Blackburn, E. H. (2001) *Cell* **106,** 661–673.
24. Prowse, K. R. & Greider, C. W. (1995) *Proc. Natl. Acad. Sci. USA* **92,** 4818–4822.
25. Kang, P. M. & Izumo, S. (2000) *Circ. Res.* **86,** 1107–1113.
26. Akli, S., Zhan, S., Abdellatif, M. & Schneider, M. D. (1999) *Circ. Res.* **85,** 319–328.
27. He, T. C., Zhou, S. B., daCosta, L. T., Yu, J., Kinzler, K. W. & Vogelstein, B. (1998) *Proc. Natl. Acad. Sci. USA* **95,** 2509–2514.
28. Sano, M., Abdellatif, M., Oh, H., Xie, M., Bagella, L., Giordano, A., Michael, L. H., DeMayo, F. J. & Schneider, M. D. (2002) *Nat. Med.* **8,** 1310–1317.
29. Counter, C. M., Avilion, A. A., LeFeuvre, C. E., Stewart, N. G., Greider, C. W., Harley, C. B. & Bacchetti, S. (1992) *EMBO J.* **11,** 1921–1929.
30. Kiaris, H. & Schally, A. V. (1999) *Proc. Natl. Acad. Sci. USA* **96,** 226–231.
31. Blasco, M. A., Funk, W., Villeponteau, B. & Greider, C. W. (1995) *Science* **269,** 1267–1270.
32. Martin-Rivera, L., Herrera, E., Albar, J. P. & Blasco, M. A. (1998) *Proc. Natl. Acad. Sci. USA* **95,** 10471–10476.
33. Multani, A. S., Ozen, M., Narayan, S., Kumar, V., Chandra, J., McConkey, D. J., Newman, R. A. & Pathak, S. (2000) *Neoplasia* **2,** 339–345.
34. Melchionna, R., Chen, X. B., Blasina, A. & McGowan, C. H. (2000) *Nat. Cell Biol.* **2,** 762–765.
35. Frey, N. & Olson, E. N. (2003) *Annu. Rev. Physiol.* **65,** 45–79.
36. Ding, B., Price, R. L., Goldsmith, E. C., Borg, T. K., Yan, X., Douglas, P. S., Weinberg, E. O., Bartunek, J., Thielen, T., Didenko, V. V. & Lorell, B. H. (2000) *Circulation* **101,** 2854–2862.
37. Ramirez, R., Carracedo, J., Jimenez, R., Canela, A., Herrera, E., Aljama, P. & Blasco, M. A. (2003) *J. Biol. Chem.* **278,** 836–842.
38. Leri, A., Franco, S., Zacheo, A., Barlucchi, L., Chimenti, S., Limana, F., Nadal-Ginard, B., Kajstura, J., Anversa, P. & Blasco, M. A. (2003) *EMBO J.* **22,** 131–139.
39. Griffith, J. D., Comeau, L., Rosenfield, S., Stansel, R. M., Bianchi, A., Moss, H. & de Lange, T. (1999) *Cell* **97,** 503–514.
40. Zhu, X. D., Kuster, B., Mann, M., Petrini, J. H. & Lange, T. (2000) *Nat. Genet.* **25,** 347–352.
41. Opresko, P. L., Von Kobbe, C., Laine, J. P., Harrigan, J., Hickson, I. D. & Bohr, V. A. (2002) *J. Biol. Chem.* **277,** 41110–41119.

Cooperative interaction of Angiopoietin-like proteins 1 and 2 in zebrafish vascular development

Yoshiaki Kubota*, Yuichi Oike*†, Shinya Satoh‡, Yoko Tabata‡, Yuichi Niikura‡, Tohru Morisada*, Masaki Akao*, Takashi Urano*, Yasuhiro Ito*, Takeshi Miyamoto*, Norihiro Nagai*, Gou Young Koh§, Sumiko Watanabe‡, and Toshio Suda*†

*Department of Cell Differentiation, The Sakaguchi Laboratory, School of Medicine, Keio University, 35 Shinanomachi, Shinjuku-ku, Tokyo 160-8582, Japan; ‡Division of Molecular and Developmental Biology, Institute of Medical Science, University of Tokyo, Minato-ku, Tokyo 108-8639, Japan; and §Biomedical Research Center and Department of Biological Sciences, Korea Advanced Institute of Science and Technology, 373-1 Guseong-dong, Yuseong-gu, Daejeon 305-701, Republic of Korea

Edited by George D. Yancopoulos, Regeneron Pharmaceuticals, Inc., Tarrytown, NY, and approved July 5, 2005 (received for review March 8, 2005)

Angiopoietin-like protein (Angptl) 1 and Angptl2, which are considered orphan ligands, are highly homologous, particularly in the fibrinogen-like domain containing the putative receptor binding site. This similarity suggests potentially cooperative functions between the two proteins. In this report, the function of Angptl1 and Angptl2 is analyzed by using morpholino antisense technology in zebrafish. Knockdown of both Angptl1 and Angptl2 produced severe vascular defects due to increased apoptosis of endothelial cells at the sprouting stage. *In vitro* studies showed that Angptl1 and Angptl2 have antiapoptotic activities through the phosphatidylinositol 3-kinase/Akt pathway, and coinjection of constitutively active Akt/protein kinase B mRNA rescued impaired vascular development seen in double knockdown embryos. These results provide a physiological demonstration of the cooperative interaction of Angptl1 and Angptl2 in endothelial cells through phosphatidylinositol 3-kinase/Akt mediated antiapoptotic activities.

angiogenesis | morpholino | phosphatidylinositol 3-kinase | Akt | apoptosis

Development of the vascular system occurs as two distinct processes, vasculogenesis and angiogenesis. In vasculogenesis, hemangioblasts derived from the lateral plate mesoderm form tubular structures of the primary vasculature. In angiogenesis, new vessels sprout from preexisting vasculature and are further remodeled to form mature blood vessels. Angiogenesis consists of several activities of endothelial cells, such as migration and apoptosis. Angiopoietin signaling through the Tie2 receptor is widely known to play a key role in angiogenesis (1–7).

Angiopoietin (Ang) 1 and all members of the angiopoietin family possess two characteristic structures: a coiled-coil domain, which likely contributes to oligomerization, and a fibrinogen-like domain, thought to contain the receptor binding site. Recently, we (8–10) and others (11–15) identified several genes encoding proteins containing both the coiled-coil domain and the fibrinogen-like domain. Although these factors were initially predicted to function as ligands for Tie receptors, they bound neither Tie1 nor Tie2. Therefore, they are currently orphan ligands and designated angiopoietin-like proteins (Angptls) or angiopoietin-related proteins (ARPs). Several studies show that Angptl/ARP family proteins possess potent activities in the vascular system (8–16). Angptl1 and Angptl2 have been reported to possess weak endothelial cell-sprouting activities (11, 12); however, there is little information as to their physiological functions.

Zebrafish offer several advantages as a model system for analyzing vascular development. One reason is that rapid external development of a transparent embryo permits visual analysis of phenotypic defects. Not only vascular structures but also apoptotic cells can be clearly visualized in whole-mount specimens (17, 18). Indeed, zebrafish has been used to investigate several vascular processes, particularly commitment of hemangioblasts (19, 20) and arterial-venous identification (21–24). Recently, we cloned the zebrafish orthologues of Angptl1 and Angptl2 (*Zangptl1* and *Zangptl2*, respectively) (25). Based on the results of a syntenic search by using the genome database and comparing expression patterns between zebrafish and mammals in adult tissues, we determined our isolated *Zangptl1* and *Zangptl2* are the orthologues of their mammalian counterparts, respectively. In that report, we also described their embryonic expression patterns. Both *Zangptl1* and *Zangptl2* are expressed mainly in the caudal part of the corpus at ≈24 h after fertilization (hpf) when angiogenesis manifested by sprouting of intersomitic vessels (ISVs) occurs. *Zangptl1* is expressed in the myotome, and *Zangptl2* is predominantly expressed in the yolk sac extension, especially in the yolk syncytial layer and the spinal cord, suggesting that both factors might act on endothelial cells of ISVs sprouting toward such structures. To examine the physiological functions of both genes simultaneously, we used a loss-of-function strategy by using morpholinos, an antisense technology widely used to knockdown multiple genes predicted to act cooperatively (26, 27). Our studies indicate that both Angptl1 and Angptl2 possess antiapoptotic activity through the phosphatidylinositol 3-kinase (PI3-K)/Akt pathway and that their cooperative activities are required for vascular development in zebrafish embryogenesis.

Materials and Methods

Zebrafish Maintenance. Zebrafish were kept at standard conditions (28). Embryos >24 hpf were raised in 0.2 mM 1-phenyl-2-thio-urea (Sigma) to prevent pigment formation.

Morpholino Sequences. Morpholinos (Gene Tools, Philomath, OR) were targeted to 25 bases around the start codons or 5′-UTR of *Zangptl1* and *Zangptl2*. They have the following sequences: the first *Zangptl1* morpholino, (Angptl1mo), 5′-CCATGCACCACGTTACACCTCTC*AT*-3′ (antisense for the start codon is underlined); 5-base mismatch morpholino of Angptl1mo (Angptl1d5), 5′-CCATcCAgCACcTTACACgTCTgAT-3′ (mismatched bases are indicated by small letters); the second *Zangptl1* morpholino, (Angptl1mo2) designed in the 5′-UTR of *Zangptl1*, 5′-TACTTCTGTTATCACCTCACAGGGT-3′; the first *Zangptl2* morpholino, (Angptl2mo), 5′-CTAGTGAAGGAACATCC*AT*GACCAC-3′ (antisense for the start codon is underlined); 5-base mismatch morpholino of

This paper was submitted directly (Track II) to the PNAS office.

Abbreviations: Ang, angiopoietin; Angptl, angiopoietin-like protein; DA, dorsal aorta; DMO, double morpholino; ERK, extracellular signal-regulated kinase; hpf, h after fertilization; HUVEC, human umbilical vein endothelial cell; ISH, *in situ* hybridization; ISV, intersomitic vessels; PKB, protein kinase B; St, standard morpholino-injected group; Zangptl*n* morphino, zebrafish orthologues of Angptl *n*.

†To whom correspondence may be addressed. E-mail: oike@sc.itc.keio.ac.jp or sudato@sc.itc.keio.ac.jp.

www.pnas.org/cgi/doi/10.1073/pnas.0501902102

Angptl2mo (Angptl2d5), 5′-CTAGTcAAcGAAgATCCATcACgAC-3′ (mismatched bases are indicated by small letters); and the second *Zangptl2* morpholino, (Angptl2mo2) designed in 5′-UTR of *Zangptl2*, 5′-CACCAGATGATCCCAGGCTATTGCA-3′.

Microinjections. Morpholinos and/or mRNA were diluted to the indicated concentrations with Danieau buffer (58 mM NaCl/0.7 mM KCl/0.4 mM $MgSO_4$/0.6 mM $Ca(NO_3)_2$/5.0 mM Hepes, pH 7.6) and ≈2 nl were injected into the yolk of one- to four-cell stage embryos. The standard control morpholino available from Gene Tools was used as an injection control.

Microangiography. Microangiography was performed as described in ref. 29. Briefly, FITC-Dextran in Danieau buffer at 2 mg/ml was injected into the sinus venosa/cardinal vein of anesthetized embryos. Photographs were taken during observation under a Leica MZFL III dissection microscope equipped with the standard FITC filter set.

Whole-Mount *in Situ* Hybridization (ISH). Probes for flk-1, fli-1, myoD, and nkx2.5 genes were cloned by PCR amplification. PCR products were subcloned into the pGEM T-easy vector. Digoxigenin (DIG)-labeled antisense RNA probes were synthesized by using a DIG RNA labeling kit (Roche Diagnostics, Mannheim, Germany). Whole-mount ISH was performed as described in ref. 30.

Whole-Mount TUNEL Staining. Embryos were fixed in 4% paraformaldehyde at 4°C overnight before staining by using the ApopTag Peroxidase *In Situ* Apoptosis Detection kit (Chemicon, Temecula, CA) according to the manufacturer's instructions, essentially as described in refs. 17 and 31.

Synthesis of Recombinant COMP-Angptl1 and -Angptl2 Proteins. To investigate the role of Angptl1 and Angptl2 directly, we generated their recombinant proteins. Notably, we designed the Angptl1 variant, COMP-Angptl1, in which the fibrinogen-like domain of mouse Angptl1 was fused to the coiled-coil domain of rat cartilage oligomeric matrix protein (DLAPQMLRELQETNAALQDVRELLRQQVKEITFLKNTVMECDACG) to avoid aggregation and insolubility of Angptl1. COMP-Angptl1 and the native form of mouse Angptl2 fused at the amino terminus to the FLAG epitope were subcloned into pCEP4 (Invitrogen, Groningen, The Netherlands), and recombinant FLAG-tagged proteins (COMP-Angptl1-FLAG and Angptl2-FLAG) were purified as described in refs. 8 and 10. The proteins obtained were visualized by Western blotting with horseradish peroxidase-conjugated anti-FLAG antibody (M2) (Sigma) (see *Supporting Materials and Methods*, which is published as supporting information on the PNAS web site).

Cell Culture. Human umbilical vein endothelial cells (HUVECs) were cultured in EGM-2 medium obtained from Cambrex (East Rutherford, NJ) as described in ref. 32. The murine pro-B cell line BaF/3 was maintained in RPMI medium 1640 (GIBCO/BRL, Grand Island, NY) supplemented with 10% FCS (GIBCO) and 1 ng/ml IL-3 (Wako, Osaka). The hepatoma line Fao was maintained in low glucose-DMEM (GIBCO/BRL) supplemented with 10% FCS.

Binding Assay. Cells were resuspended and incubated in PBS with 5% FCS including either FLAG-tagged or biotinylated COMP-Angptl1 and Angptl2 for 30 min on ice. In some experiments, cells were preincubated in PBS with 5% FCS including indicated proteins at the same concentration for 15 min on ice before the primary incubation. Immunodetection of cells bound by COMP-Angtl1 or -Angptl2 was accomplished with FITC-conjugated anti-FLAG antibody or Streptavidin. Stained cells were analyzed by using a FACScan cytometer and CELLQUEST software (Becton Dickinson, Franklin Lakes, NJ), and the mean fluorescent intensity was monitored and calculated as the ratio in comparison with the vehicle-treated cells.

Phosphorylation Assay of Extracellular Signal-Regulated Kinase (ERK)1/2 and Akt. Cells were starved in their respective maintenance medium without serum and growth factors for 12 h (HUVECs and Fao) or 4 h (BaF/3) and stimulated with 0.5 μg/ml COMP-Angptl1 or -Angptl2 proteins for various times. Phosphorylation assays of ERK1/2 and Akt were performed as described in ref. 32.

TUNEL Assay of HUVECs. For TUNEL assays, HUVECs were cultured in serum-free medium in the presence of either vehicle (PBS) or 0.5 μg/ml COMP-Angptl1 or -Angptl2. In some experiments, cells were incubated with the MEK inhibitor, PD980059 (Biomol, Plymouth Meeting, PA) (5 μg/ml) or the PI3-K inhibitor, LY294002 (Calbiochem, San Diego) (5 μg/ml). As controls in the inhibitor experiments, equivalent amounts of DMSO vehicle were added to the medium. Apoptotic adherent cells were stained by using an ApopTag Fluorescein *In Situ* Apoptosis Detection Kit (Chemicon). Nuclear staining was done by TOTO3. Cells were observed under a fluorescent microscope.

Synthesis of Myristoylated Akt/Protein Kinase B (PKB) mRNA. To prepare the active form of Akt-1/PKBα mRNA, myristoylated human AKT-1/PKBα cDNA (kindly provided by Dr. Kenneth Walsh, Boston University, Boston), which has been reported to have high homology with a zebrafish orthologue and function in zebrafish *in vivo* (17), was linearized at the 3′ end, and capped RNAs were *in vitro* transcribed by using the Message Machine Kit (Ambion, Austin, TX) as described in refs. 17 and 33.

Results

Loss of Angptl1 and Angptl2 Promotes Vascular Defects. To evaluate the physiological effect of Angptl1 and Angptl2, we undertook loss-of-function experiments in zebrafish by using morpholinos. Our first observation was embryonic lethality at 72 hpf caused by pericardial effusion. Although the number of embryos with pericardial effusion showed a dose-dependent increase in the Angptl1mo- (Angptl1MO) and Angptl2mo- (Angptl2MO) injected group compared with the standard morpholino-injected group (St), the group injected with both Angptl1mo and Angptl2mo (double morpholino, DMO) showed remarkable increases in the number of embryos with pericardial effusion (Fig. 1*A*; see also Fig. 5, which is published as supporting information on the PNAS web site). To determine whether defects in heart development occurred at earlier stages, we examined expression of *nkx2.5* and found normal expression in DMO embryos (Fig. 6, which is published as supporting information on the PNAS web site). At 48 hpf, when the heartbeat can be easily observed, the DMO group showed a normal heartbeat similar to the St group (Movies 1 and 2, which are published as supporting information on the PNAS web site). To determine whether pericardial effusion was attributable to defects in vascular development, we observed blood flow in the same embryos. Interestingly, although we detected blood flow in two major trunk vessels, the dorsal aorta (DA) and postcardinal vein, in both St and DMO groups, we could not detect blood flow in ISVs and the dorsal-longitudinal anastomosus vessel in the DMO group as detected in the St group (Movies 3 and 4, which are published as supporting information on the PNAS web site), suggesting that vascular defects precede heart defects. To visualize blood vessel formation at this stage, we performed angiography (Fig. 1*B*) and ISH for fli-1 (Fig. 1*C*). Although the major trunk vessels were clearly detected, ISVs and dorsal-longitudinal

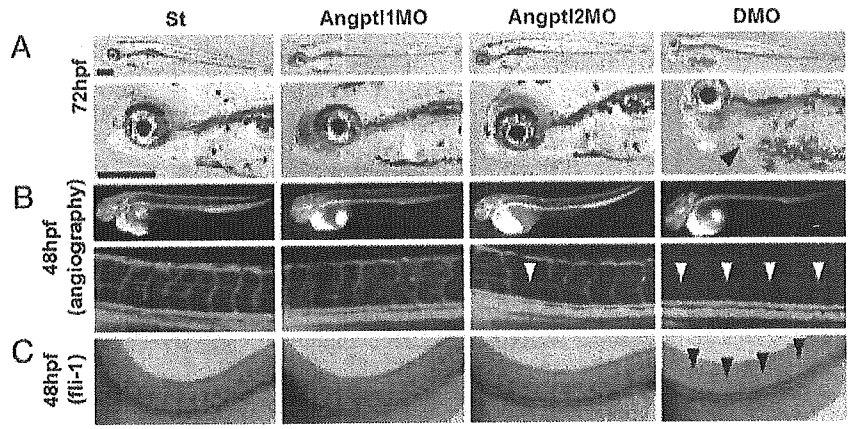

Fig. 1. Vascular defects observed in Angptl1 and Angptl2 double knockdown embryos. (*A*) Representative photographs of simple microscopic observation of 72 hpf embryos St, Angptl1MO, Angptl2MO, and DMO groups. The lower four photographs are high magnifications of the upper four. A closed arrowhead indicates pericardial effusion seen especially in DMO groups (Scale bar: 400 μm.). (*B*) Representative photographs of angiography at 48 hpf. The lower four photographs are high magnifications of the upper four. Open arrowheads indicate the absence of blood flow in ISVs and dorsal-longitudinal anastomosus vessels. (*C*) Representative photographs of whole-mount ISH of fli-1 at 48 hpf. Filled arrowheads indicate absence of ISVs and dorsal-longitudinal anastomosus vessels in DMO.

anastomosus vessels was undetectable in the DMO group in both experiments. These findings suggest that impaired vascular development is the primary defect seen when Angptl1 and Angptl2 activity is lost.

Loss of Angptl1 and Angptl2 Promotes Impaired Sprouting of ISVs and Increased Numbers of Apoptotic Cells Around DA. To determine the initiation of vascular defects in DMO, we examined vascular development at early developmental stages by whole-mount ISH of endothelial markers. Vascular defects were first observed as impaired sprouting of ISVs as detected by ISH of flk-1 at 28 hpf. The DMO group showed complete loss of sprouting of ISVs (Fig. 2*A*). Defects of impaired sprouting vessels were quantitatively analyzed as described in refs. 18 and 27. A high percentage of the DMO group showed impaired sprouting (Fig. 7, which is published as supporting information on the PNAS web site). To confirm the specificity of these findings, we analyzed defects of sprouting vessels by using second morpholinos or morpholinos with five mismatched bases as negative controls (Fig. 8 and 9, which are published as supporting information on the PNAS web site). In both experiments, we obtained results similar to those seen with the first set of morpholinos.

The formation of hemangioblasts is a very early step in the development of the vascular system. Hemangioblasts form in the lateral plate mesoderm at 12 hpf, and tubular structures of the primary vasculature formed by the hemangioblasts at 18 hpf can be visualized by ISH of fli-1 and flk-1. Formation of such structures was normal in DMO embryos, suggesting normal

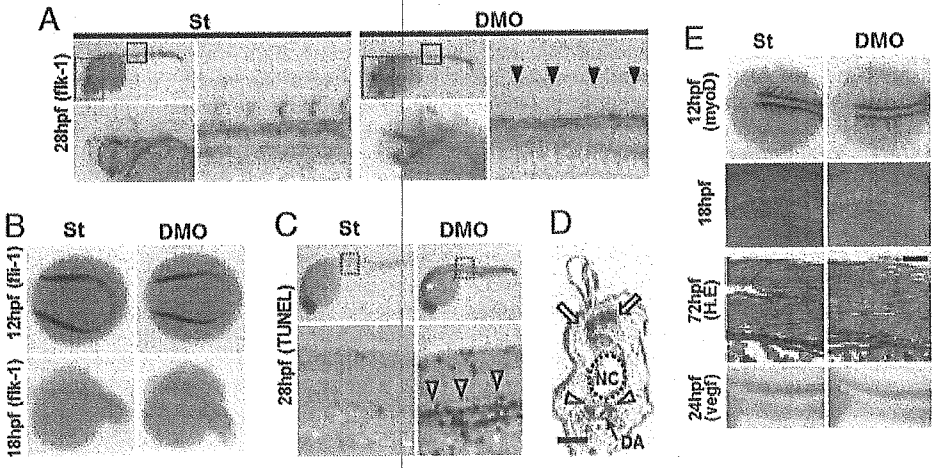

Fig. 2. Impaired sprouting of ISVs and elevated apoptotic cells around the DA are seen in DMO embryos. (*A*) Representative photographs of whole-mount ISH of flk-1 at 28 hpf in St and DMO embryos. High magnification images of head portions indicated by dotted grids in the upper left are shown in the lower left. Normal vasculature in head portion is seen in both St and DMO. High magnification images in the trunks indicated by closed grids in the upper left are shown in the right images. Filled arrowheads indicate ISVs with impaired sprouting in DMO. (*B*) Representative photographs of whole-mount ISH of fli-1 at 12 hpf and flk-1 at 18 hpf in St and DMO embryos. Normal vasculogenesis occurs in DMO-injected embryos. (*C*) Representative photographs of whole-mount TUNEL assay at 28 hpf. High magnification images of the trunk indicated by dotted grids in *Upper* are shown in *Lower*. Open arrowheads indicate increased apoptotic cells in the area of major trunk vessels in DMO. (*D*) A sagittal section of DMO embryos stained with TUNEL. Open arrowheads indicate apoptotic cells around the DA, and open arrows indicate naturally occurring apoptosis in the neural tube. NC, notochord. (Scale bar: 50 μm.). (*E*) Representative photographs of somites examined by whole-mount ISH of myoD at 12 hpf, simple microscopic observation at 18 hpf, hematoxylin/eosin staining of sagittal sections at 72 hpf, and whole-mount ISH of vegf at 24 hpf. Somitogenesis and vegf expression are not impaired in DMO embryos. (Scale bar: 100 μm.).

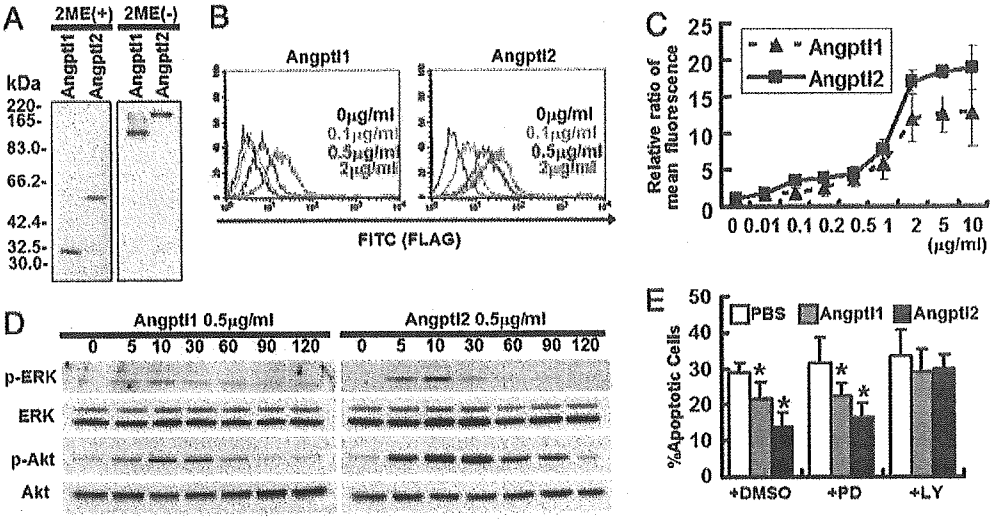

Fig. 3. Angptl1 and Angptl2 bind to endothelial cells, and possess antiapoptotic activity through the PI3-K/Akt pathway. (*A*) Western blotting analysis with an anti-FLAG antibody with (*Left*) or without (*Right*) 2-mercaptoethanol (2ME). (*B* and *C*) Binding of COMP-Angptl1-FLAG and Angptl2-FLAG to HUVECs. The FITC intensity indicates cells bound by FLAG-tagged proteins. With both COMP-Angptl1 (*Left*) and Angptl2 (*Right*), intensities increased in a dose-dependent manner with saturation at ≈2 μg/ml. (*D*) Phosphorylation assay of ERK1/2 and Akt. HUVECs were treated with COMP-Angptl1 or -Angptl2 proteins. Immunoblotting was performed with anti-pERK1/2 or anti-pAkt antibody. Total amounts of ERK1/2 or Akt proteins were monitored by reprobing membranes with anti-ERK1/2 antibody and anti-Akt antibody. (*E*) TUNEL assay. HUVECs were cultured in the presence of either vehicle (PBS) or 0.5 μg/ml of COMP-Angptl1 or -Angptl2. In some experiments, cells were incubated with DMSO or 5 μg/ml PD980059 or LY294002. Data shown is the average of 6 fields each in six independent experiments ($n = 36$). *, $P < 0.03$ (compared with PBS in each group).

vasculogenesis can occur in the absence of Angptl1 and Angptl2 (Fig. 2*B*).

To investigate the mechanism underlying impaired sprouting, we examined apoptotic cells *in vivo* by whole-mount TUNEL assay. Apoptotic cells around the DA were markedly increased in the DMO group compared with the control group (Fig. 2 C and *D*). On the other hand, there was no significant difference in the number of physiological apoptotic cells in neural tube (31) between St and DMO groups when we counted TUNEL-positive cells in the neural tube within rostral and caudal ends of yolk sac extension (17.9 ± 5.34 and 19.8 ± 5.3, respectively: $n = 7$, $P = 0.53$).

Because somitic cells secrete angiogenic factors such as VEGF, normal development of somites is essential for angiogenesis in zebrafish. Thus, we examined somitogenesis and VEGF expression in the DMO group. Somitogenesis appeared normal and no alteration in VEGF expression was observed in the DMO group (Fig. 2*E*). These results show that the loss of Angptl1 and Angptl2 promotes impaired sprouting of ISVs and increased apoptotic cells around the DA.

Angptl1 and Angptl2 Bind to Endothelial Cells. To clarify the mechanism underlying the *in vivo* phenotype seen in zebrafish after DMO treatment, we performed *in vitro* studies by using HUVECs. First, we generated FLAG-tagged mouse COMP-Angptl1 and -Angptl2 proteins. Although we successfully synthesized the native form of Angptl2, we failed to purify that of Angptl1 because of its unique tendency to aggregate and become insoluble. Although similar difficulties purifying Ang1 have been reported, by replacing the N-terminal portion of Ang1 with a minimal coiled-coil domain from cartilage oligomeric matrix protein (COMP), Koh *et al.* (34, 35) have succeeded in generating a soluble, stable, and potent Ang1 variant, COMP-Ang1 protein. Using the same strategy, we succeeded in generating a soluble and stable Angptl1 variant, COMP-Angptl1. First, we observed monomeric forms of COMP-Angptl1 and -Angptl2 in the presence of reducing agents, 2-mercaptoethanol (2ME), and multimeric forms in nonreducing conditions without 2-mercaptoethanol by Western blotting with an anti-FLAG antibody (Fig. 3*A*). Moreover, we found that COMP-Angptl1 and Angptl2 bound neither Tie1 nor Tie2 (data not shown).

Next, we found that COMP-Angptl1 and Angptl2 show specific binding to HUVECs by FACS analysis. Dose–response binding curves, saturation of binding at a concentration (Fig. 3 *B* and *C*), and greatly decreased binding to other cell types like BaF/3 and Fao (Fig. 10, which is published as supporting information on the PNAS web site) suggested that binding between HUVECs and both proteins was specific, and that the affinity of Angptl2 for HUVECs was greater than that of COMP-Angptl1.

The amino acid sequences of Angptl1 and Angptl2 are very similar between mammalian and zebrafish proteins. Homology is particularly high in the fibrinogen-like domain (Fig. 11, which is published as supporting information on the PNAS web site). Such homology, combined with the fact that the *in vivo* phenotype in zebrafish was particularly robust in double knockdown embryos, suggested a cooperative role of Angptl1 and Angptl2, most likely through a putative common receptor. When HUVECs were pretreated with Angptl2-FLAG, binding of biotinylated COMP-Angptl1 on HUVECs was completely inhibited. In parallel, similar, but partial, inhibition of binding between COMP-Angptl1-FLAG and HUVECs was observed when the converse experiments were performed, (Fig. 12, which is published as supporting information on the PNAS web site). These findings may support a possibility of the cooperative function of Angptl1 and Angptl2 through a common receptor, although further analysis for identifying their cognate receptor will be necessary.

Angptl1 and Angptl2 Possess Antiapoptotic Activity Through the PI3-K/Akt Pathway. When HUVECs were treated with COMP-Angptl1 or Angptl2, phosphorylation of ERK1/2 and Akt was observed, peaking 10 min after treatment (Fig. 3*D*). No effect on BaF/3 and Fao cells was detected (Fig. 13, which is published as supporting information on the PNAS web site). Furthermore, no effect on p38 MAPK and JNK in HUVECs was seen (data not shown). We next examined the biological activities of COMP-Angptl1 and -Angptl2 on HUVECs. Because the ERK1/2

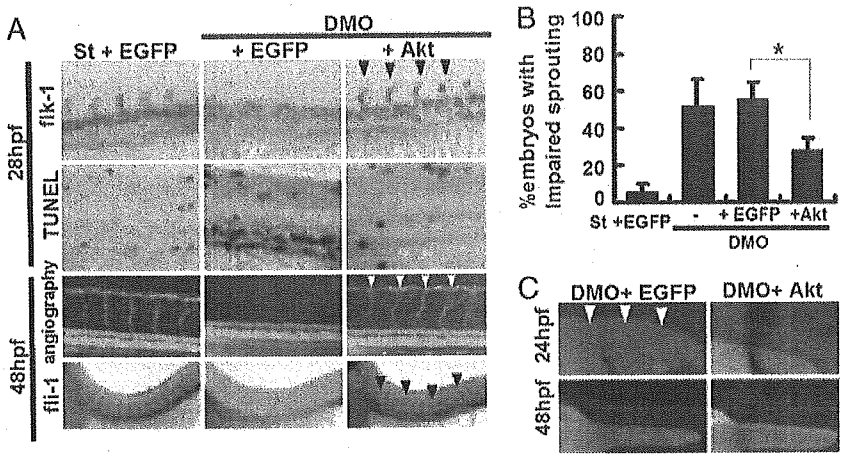

Fig. 4. Coinjection of myristoylated Akt rescues vascular defects in DMO embryos. (*A*) Representative photographs of whole-mount ISH of flk-1 at 28 hpf, whole-mount TUNEL assay at 28 hpf, angiography at 48 hpf, and ISH of fli-1 at 48 hpf. Fifty picograms of EGFP mRNA or myr-Akt mRNA was coinjected into DMO (2 ng each of Angptl1mo and Angptl2mo). As a control, we coinjected 50 pg of EGFP mRNA with 4 ng of the standard morpholino (St plus EGFP). Rescued blood vessels are indicated by filled arrowheads and open arrowheads. (*B*) Percentages of embryos with impaired sprouting of ISVs in five independent experiments ($n = 31–42$ in each experiment) *, $P < 0.01$. (*C*) EGFP activity in the EGFP coinjected group (*Left*) and the myr-Akt coinjected group (*Right*) at 24 hpf and 48 hpf. Open arrowheads indicate abundant EGFP expression in the trunk of an embryo at 24 hpf.

pathway is a major intracellular signaling pathway activated by factors that promote endothelial proliferation, we examined proliferative activity by BrdUrd incorporation. Although VEGF used as a control significantly promoted BrdUrd incorporation, neither COMP-Angptl1 nor Angptl2 stimulated significant increases in BrdUrd incorporation (Fig. 14, which is published as supporting information on the PNAS web site). We next examined antiapoptotic activity of COMP-Angptl1 and -Angptl2 on HUVECs. The numbers of apoptotic cells were significantly decreased in both COMP-Angptl1 and -Angptl2-treated groups based on TUNEL assays (Fig. 3*E*) and Annexin V assays (Fig. 15, which is published as supporting information on the PNAS web site). Finally, to evaluate whether MEK or PI3-K is involved in the antiapoptotic activity of COMP-Angptl1 and -Angptl2, we reexamined apoptotic activity in the presence of their respective inhibitors, PD98059 or LY294002. As compared with controls treated with equivalent amounts of DMSO, LY294002, but not PD98059, significantly inhibited antiapoptotic activity of Comp-Angptl1 and Angptl2 as seen in TUNEL and AnnexinV assays (Figs. 3*E* and 15). These findings suggest that antiapoptotic activity on HUVECs induced by COMP-Angptl1 and -Angptl2 is mediated by the PI3-K/Akt pathway.

Coinjection of Constitutive Active Akt Rescues Vascular Defects Induced by Loss of Angptl1 and Angptl2. Based on our *in vitro* studies, we examined whether activation of Akt by coinjection of myristoylated Akt-1/PKBα mRNA (myr-Akt) rescued the vascular defects seen in DMO embryos. First, by titration experiments, we found a 50-pg injection was the appropriate dose for rescue experiments. Higher doses of Akt mRNA produced severe defects leading to early lethality (data not shown). At the optimal dose, up-regulated Akt/PKB activity rescued impaired angiogenesis seen in the DMO group. As a control, coinjection of the equivalent amount of EGFP mRNA did not rescue defects (Fig. 4 *A* and *B*). Although coinjected EGFP activity was almost undetectable at 48 hpf, we detected abundant EGFP expression in the trunks of embryos at 24 hpf (Fig. 4*C*), suggesting that myr-Akt mRNA is likely active at 24 hpf when sprouting of ISVs occurs.

Discussion

In previous reports, Angptl1 and Angptl2 were shown to possess pro- or antiangiogenic activity. However, there are few reports regarding the physiological role of either protein *in vivo*. In this report, a morpholino antisense strategy in zebrafish showed that Angptl1 and Angptl2 function cooperatively in embryonic angiogenesis through antiapoptotic activity. In addition, both Angptl1 and Angptl2 activate PI3-K/Akt and inhibit apoptosis in cultured endothelial cells. Furthermore, we showed that activation of Akt could rescue the vascular defects induced by loss of Angptl1 and Angptl2.

Recently, we showed that in zebrafish *Zangptl1* is expressed in the myotome, and *Zangptl2* is expressed mainly in the spinal cord and yolk syncytial layer at the time angiogenesis occurs (25). In this report, we demonstrate that loss of function of both proteins leads to vascular defects, specifically in the sprouting of ISVs. ISVs sprout and extend toward the dorsal side of embryos between the myotome and spinal cord. Therefore, one hypothesis is that Angptl1 and Angptl2 secreted from nearby structures acts together on endothelial cells of ISVs as survival factors through activation of the PI3-K/Akt pathway.

In initial reports, Kim *et al.* (11, 12) reported that both Angptl1 and Angptl2 have significant but weak endothelial cell-sprouting activities *in vitro*. Later, it was reported that Angptl1 inhibited VEGF-induced angiogenesis, and it was thus named "Angioarrestin" (16). These authors also proposed that not only Angptl1 but Angptl2 might be antiangiogenic factors. In our hands, Angptl1 stimulated phosphorylation of ERK1/2 and Akt and had significant antiapoptotic activity on HUVECs. Angptl1 may function as either a pro- or antiangiogenic factor, depending on cell context, and it is possible that the primary function of Angptl1 on endothelial cells is an antiapoptotic activity, not an effect on proliferation and sprouting. Our *in vivo* results obtained in zebrafish support that hypothesis: minor vascular defects were seen in Angptl2 knockdown embryos, whereas Angptl1 knockdown embryos showed few vascular abnormalities. Based on the severe defects seen in double knockdown embryos, we suggest that Angptl1 may play a regulatory role for the dominant function of Angptl2 in the process of angiogenesis; Angptl1 may exhibit proangiogenic activity particularly in the absence of Angptl2.

Angiopoietins have been shown to play critical antiapoptotic roles in mammals, similar to findings reported here concerning zebrafish Angptl1 and Angptl2. Our findings prompted us to initiate comparative studies between Angiopoietins and Angptl

families. The genes encoding zebrafish Ang1 (*Zang1*) and Ang2 (*Zang2*) are expressed in the mesenchyme surrounding major trunk vessels (36). Notably, zebrafish Tie-2 is abundantly expressed in postcardinal vein, but not in the DA (37), whereas differences of expression patterns of Tie2 between the DA and postcardinal vein are not seen in mammals. Our data in zebrafish shows that the effect of loss of Angptl1 and Angptl2 was predominantly in arterial angiogenesis. It is important to determine whether Angiopoietin and Angptl signaling are transduced differentially in arterial and venous angiogenesis in zebrafish.

In conclusion, we have shown that the cooperative interactions of Angptl1 and Angptl2 are required for vascular development of zebrafish *in vivo*. We have also shown that Angptl1 and Angptl2 bind to the endothelial cells and both have antiapoptotic activities through the PI3-K/Akt pathway *in vitro*. Identification of a receptor of Angptl1 and Angptl2 is essential for the further analysis of the functional relationships between Angiopoietins and Angptls.

This work was supported by grants-in-aid from the Human Frontiers Science Promotion and the Ministry of Education, Culture, Sports, Science, and Technology of Japan, by a research grant from the Mochida Memorial Foundation for Medical and Pharmaceutical Research, and by a Keio University grant-in-aid for Encouragement of Young Medical Students.

1. Suri, C., Jones, P. F., Patan, S., Bartunkova, S., Maisonpierre, P., Davis, S., Sato, T. N. & Yancopoulos, G. D. (1996) *Cell* **87,** 1171–1180.
2. Sato, T. N., Tozawa, Y., Deutsch, U., Wolburg-Buchholz, K., Fujiwara, Y., Gendron-Maguire, M., Grigley, T., Wolburg, H., Risau, W. & Qin, Y. (1995) *Nature* **376,** 70–74.
3. Lobov, I. B., Brooks, P. C. & Lang, R. A. (2002) *Proc. Natl. Acad. Sci. USA.* **99,** 11205–11210.
4. Koblizek, T. I., Weiss, C., Yancopoulos, G. D., Deutsch, U. & Risau, W. (1998) *Curr. Biol.* **8,** 529–532.
5. Witzenbichler, B., Maisonpierre, P. C., Jones, P., Yancopoulos, G. D. & Isner, J. M. (1998) *J. Biol. Chem.* **273,** 18514–18521.
6. Papapetropoulos, A., Garcia-Cardena, G., Dengler, T. J., Maisonpierre, P. C., Yancopoulos, G. D. & Sessa, W. C. (1999) *Lab. Invest.* **79,** 213–223.
7. Kwak, H. J., So, J.-N., Lee, S. J., Kim, I. & Koh, G. Y. (1999) *FEBS Lett.* **448,** 249–253.
8. Ito, Y., Oike, Y., Yasunaga, K., Hamada, K., Miyata, K., Matsumoto, S., Sugano, S., Tanihara, H., Masuho, Y. & Suda, T. (2003) *Cancer Res.* **63,** 6651–6657.
9. Oike, Y., Yasunaga, K., Ito, Y., Matsumoto, S., Maekawa, H., Morisada, T., Arai, F., Nakagata, N., Takeya, M., Masuho, Y. & Suda, T. (2003) *Proc. Natl. Acad. Sci. USA* **100,** 9494–9499.
10. Oike, Y., Ito, Y., Maekawa, H., Morisada, T., Kubota, Y., Akao, M., Urano, T., Yasunaga, K. & Suda, T. (2004) *Blood* **103,** 3760–3765.
11. Kim, I., Kwak, H. J., Ahn, J. E., So, J. N., Liu, M., Koh, K. N. & Koh, G. Y. (1999) *FEBS Lett.* **443,** 353–356.
12. Kim, I., Moon, S. O., Koh, K. N., Kim, H., Uhm, C. S., Kwak, H. J., Kim, N. G. & Koh, G. Y. (1999) *J. Biol. Chem.* **274,** 26523–26528.
13. Kim, I., Kim, H. G., Kim, H., Kim, H. H., Park, S. K., Uhm, C. S., Lee, Z. H. & Koh, G. Y. (2000) *Biochem. J.* **346,** 603–610.
14. Camenisch, G., Pisabarro, M. T., Sherman, D., Kowalski, J., Nagel, M., Hass, P., Xie, M. H., Gurney, A., Bodary, S., Liang, X. H., *et al.* (2002) *J. Biol. Chem.* **277,** 17281–17290.
15. Le Jan, S., Amy, C., Cazes, A., Monnot, C., Lamande, N., Favier, J., Philippe, J., Sibony, M., Gasc, J. M., Corvol, P., *et al.* (2003) *Am. J. Pathol.* **162,** 1521–1528.
16. Dhanabal, M., LaRochelle, W. J., Jeffers, M., Herrmann, J., Rastelli, L., McDonald, W. F., Chillakuru, R. A., Yang, M., Boldog, F. L., Padigaru, M., *et al.* (2002) *Cancer Res.* **62,** 3834–3841.
17. Chan, J., Bayliss, P. E., Wood, J. M. & Roberts, T. M. (2002) *Cancer Cell* **1,** 257–267.
18. Lee, P., Goishi, K., Davidson, A. J., Mannix, R., Zon, L. & Klagsbrun, M. (2002) *Proc. Natl. Acad. Sci. USA* **99,** 10470–10475.
19. Liao, W., Bisgrove, B. W., Sawyer, H., Hug, B., Bell, B., Peters, K., Grunwald, D. J. & Stainier, D. Y. (1997) *Development (Cambridge, U.K.)* **124,** 381–389.
20. Liao, E. C., Paw, B. H., Oates, A. C., Pratt, S. J., Postlethwait, J. H.& Zon, L. I. (1998) *Genes Dev.* **12,** 621–626.
21. Zhong, T. P., Childs, S., Leu, J. P. & Fishman, M. C. (2001) *Nature* **414,** 216–220.
22. Zhong, T. P., Rosenberg, M., Mohideen, M. A., Weinstein, B. M. & Fishman, M. C. (2000) *Science* **287,** 1820–1824.
23. Lawson, N. D., Vogel, A. M. & Weinstein, B. M. (2002) *Dev. Cell* **3,** 127–136.
24. Lawson, N. D., Scheer, N., Pham, V. N., Kim, C. H. & Chitnis, A. B. (2001) *Development (Cambridge, U.K.)* **128,** 3675–3683.
25. Kubota, Y., Oike, Y., Satoh, S., Tabata, Y., Niikura, Y., Morisada, T., Akao, M., Urano, T., Ito, Y., Miyamoto, T., *et al.* (2005) *Gene Expr. Patterns* **5,** 679–685.
26. Nasevicius, A. & Ekker, S. C. (2000) *Nat. Genet.* **26,** 216–220.
27. Chen, E., Hermanson, S. & Ekker, S. C. (2004) *Blood* **103,** 1710–1719.
28. Westerfield, M. (1994) *The Zebrafish Book: A Guide for the Laboratory Use of Zebrafish* (University of Oregon Press, Eugene, OR).
29. Nasevicius, A., Larson, J. & Ekker, S. C. (2000) *Yeast* **17,** 294–301.
30. Jowett, T. (1999) *Methods Cell. Biol.* **59,** 63–85.
31. Abdelilah, S., Mountcastle-Shah, E., Harvey, M., Solnica-Krezel, L., Schier, A. F., Stemple, D. L., Malicki, J., Neuhauss, S. C., Zwartkruis, F., Stainier, D. Y., *et al.* (1996) *Development (Cambridge, U.K.)* **123,** 217–227.
32. Maekawa, H., Oike, Y., Kanda, S., Ito, Y., Yamada, Y., Kurihara, H., Nagai, R. & Suda T. (2003) *Arterioscler. Thromb. Vasc. Biol.* **23,** 2008–2014.
33. Ramaswamy, S., Nakamura, N., Vazquez, F., Batt, D. B., Perera, S., Roberts, T. M. & Sellers, W. R. (1999) *Proc. Natl. Acad. Sci. USA* **96,** 2110–2115.
34. Cho, C.-H., Kammerer, R. A., Lee, H. J., Steinmetz, M. O., Ryu, Y. S., Lee, S. H., Yasunaga, K., Kim, K.-T., Kim, I., Choi, H.-H., *et al.* (2004) *Proc. Natl. Acad. Sci. USA* **101,** 5547–5552.
35. Cho, C.-H., Kammerer, R. A., Lee, H. J., Yasunaga, K., Kim, K.-T., Choi, H.-H., Kim, W., Kim, S. H., Park, S. K., Lee, G. M. & Koh, G. Y. (2004) *Proc. Natl. Acad. Sci. USA* **101,** 5553–5558.
36. Pham, V. N., Roman, B. L. & Weinstein, B. M. (2001) *Dev. Dyn.* **221,** 470–474.
37. Lyons, M. S., Bell, B., Stainier, D. & Peters, K. G. (1998) *Dev. Dyn.* **212,** 133–140.

nature medicine

Angiopoietin-related growth factor antagonizes obesity and insulin resistance

Yuichi Oike[1], Masaki Akao[1], Kunio Yasunaga[2], Toshimasa Yamauchi[3], Tohru Morisada[1], Yasuhiro Ito[1], Takashi Urano[1], Yoshishige Kimura[1], Yoshiaki Kubota[1], Hiromitsu Maekawa[1], Takeshi Miyamoto[1], Keishi Miyata[1], Shun-ichiro Matsumoto[2], Juro Sakai[4], Naomi Nakagata[5], Motohiro Takeya[6], Haruhiko Koseki[7], Yoshihiro Ogawa[8], Takashi Kadowaki[3] & Toshio Suda[1]

Angiopoietin-related growth factor (AGF), a member of the angiopoietin-like protein (Angptl) family, is secreted predominantly from the liver into the systemic circulation. Here, we show that most (>80%) of the AGF-deficient mice die at about embryonic day 13, whereas the surviving AGF-deficient mice develop marked obesity, lipid accumulation in skeletal muscle and liver, and insulin resistance accompanied by reduced energy expenditure relative to controls. In parallel, mice with targeted activation of AGF show leanness and increased insulin sensitivity resulting from increased energy expenditure. They are also protected from high-fat diet–induced obesity, insulin resistance and nonadipose tissue steatosis. Hepatic overexpression of AGF by adenoviral transduction, which leads to an approximately 2.5-fold increase in serum AGF concentrations, results in a significant ($P < 0.01$) body weight loss and increases insulin sensitivity in mice fed a high-fat diet. This study establishes AGF as a new hepatocyte-derived circulating factor that counteracts obesity and related insulin resistance.

Obesity is an increasingly prevalent medical and social problem with potentially devastating consequences because it clusters with type 2 diabetes, hypertension and hyperlipidemia in the metabolic syndrome or syndrome X[1,2]. The molecular mechanisms underlying obesity have not been fully clarified, and effective therapeutic approaches are currently of general interest. Inhibition of weight gain requires that we burn more calories than we take in. From this perspective, adaptive thermogenesis, which is the process of heat production in response to diet or environment temperature, is an important defense against obesity[3,4].

Recently, we and several groups independently identified several molecules containing a coiled-coil domain and a fibrinogen-like domain, motifs structurally conserved in angiopoietins[5,6]. Because these molecules do not bind the angiopoietin receptor, Tie-2, they were named angiopoietin-like proteins (Angptl). We identified angiopoietin-related growth factor (AGF, also known as Angptl6 and encoded by the gene *Angptl6*) as a member of the Angptl family and showed that it is a circulating orphan peptide secreted by liver that induces angiogenesis and proliferation of skin cells, and thereby promotes wound healing[6–8]. Furthermore, several early reports have indicated that there are additional members of the Angptl family, which are currently considered orphan ligands, as angiogenic factors in the vascular system[6,9–11]. On the other hand, several reports indicate that Angptls have biological effects on nonvascular cells. For example, Angptl4 (refs. 12,13; also known as PGAR and FIAF) and Angptl3 (refs. 14,15) regulate fat and/or lipid metabolic homeostasis in addition to controlling angiogenesis[10,11]. These findings suggest that Angptls exert multiple biological functions; however, the physiological and pathological roles of each member of the Angptls have not been fully clarified.

Here we show that most (>80%) of the mice with mutations in AGF (*Angptl6*$^{-/-}$ mice) die at about embryonic day 13, with apparent cardiovascular defects including poorly formed yolk sac and vitelline vessels. Notably, the surviving *Angptl6*$^{-/-}$ mice become markedly obese and have obesity-related metabolic disorders. In parallel, mice with targeted activation of AGF *in vivo* (*Angptl6*-transgenic mice) show markedly reduced adiposity and insulin sensitivity. Furthermore, *Angptl6*-transgenic mice are completely resistant to high-fat diet–induced obesity and impaired insulin sensitivity. Moreover, we found that hepatic overexpression of AGF by adenoviral transduction, which leads to an approximately 2.5-fold increase in serum AGF concentrations, results in a significant ($P < 0.01$) body weight loss and ameliorates insulin sensitivity in mice fed a high-fat diet. Based on these findings, we report here that AGF is a new hepatocyte-derived circulating factor counteracting high-fat diet–induced obesity and related insulin resistance through increased energy expenditure, thereby suggesting a therapeutic potential in counteracting obesity and diabetes.

[1]Department of Cell Differentiation, The Sakaguchi Laboratory, School of Medicine, Keio University, 35 Shinanomachi, Shinjuku-ku, Tokyo 160-8582, Japan. [2]Molecular Medicine Laboratories, Yamanouchi Pharmaceutical Co., Ltd., Tsukuba, 305-8585, Japan. [3]Department of Internal Medicine, Graduate School of Medicine, University of Tokyo, Tokyo 113-8655, Japan. [4]Research Center for Advanced Science and Technology, University of Tokyo, Tokyo 153-8904, Japan. [5]Center for Animal Resources and Development, and [6]Department of Pathology, Kumamoto University, Kumamoto 860-0811, Japan. [7]RIKEN Research Center for Allergy and Immunology, Tsurumi-ku, Yokohama 230-0045, Japan. [8]Department of Molecular Medicine and Metabolism, Medical Research Institute, Tokyo Medical and Dental University, Tokyo 101-0062, Japan. Correspondence should be addressed to Y.O. (oike@sc.itc.keio.ac.jp).

Published online 20 March 2005; doi:10.1038/nm1214

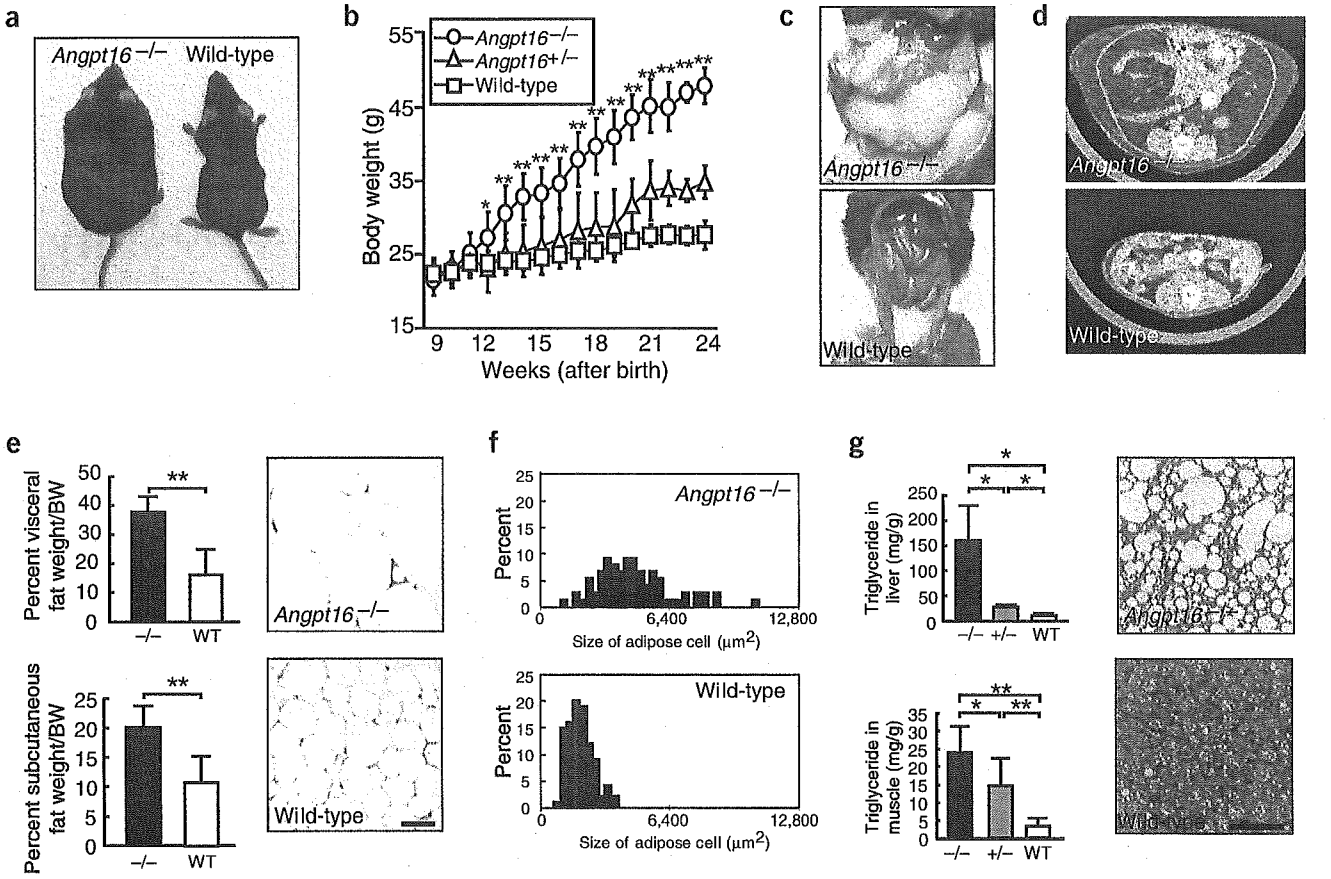

Figure 1 Obesity in *Angptl6*$^{-/-}$ mice on a normal diet. (**a**) Gross appearance of *Angptl6*$^{-/-}$ mice and wild-type control mice. (**b**) Body weight of each genotype ($n = 8$). (**c**–**g**) Abdominal cavity (**c**), CT findings at a level of 8 mm above the top of the iliac bone (**d**), visceral fat ($n = 5$) and subcutaneous fat ($n = 5$) weight/body weight, and histological analysis (**e**) and distribution of cell size (**f**) of WAT of *Angptl6*$^{-/-}$ mice and wild-type mice. (**g**) Triglyceride levels in liver ($n = 5$) and gastrocnemius muscle ($n = 5$), and hematoxylin and eosin–stained sections of BAT of *Angptl6*$^{-/-}$ and wild-type mice. Data are mean ± s.d. Bars in histological sections indicate 50 μm. $^{*}P < 0.05$, $^{**}P < 0.01$, between the two genotypes indicated. Female mice 8 months after birth were used for all experiments.

RESULTS

Disruption of *Angptl6 in vivo*

To investigate the physiological role of AGF, we generated mice with mutations in *Angptl6* (**Supplementary Fig. 1** online). Most (>80%) of *Angptl6*$^{-/-}$ mice die at approximately embryonic day 13 (**Supplementary Fig. 1**), with apparent cardiovascular defects including poorly formed yolk sac and vitelline vessels (data not shown). Notably, the surviving *Angptl6*$^{-/-}$ mice become markedly obese even on a normal chow diet, suggesting that AGF has a crucial role in regulating adiposity in adulthood (**Fig. 1a**). We therefore focused on how AGF functions in the pathogenesis of obesity and associated disorders.

Obesity in *Angptl6*$^{-/-}$ mice

Twelve weeks after birth, *Angptl6*$^{-/-}$ mice showed increases in body weight that surpassed those seen in wild-type (*Angptl6*$^{+/+}$) mice on a normal chow diet (**Fig. 1b**). There were no phenotypic differences between male and female mice. Macroscopic and computed tomographic (CT) analyses taken 8 months after birth showed that both visceral and subcutaneous fat depots were significantly increased in *Angptl6*$^{-/-}$ mice compared to wild-type mice (**Fig. 1c–e**). Sections of white adipose tissue (WAT) from *Angptl6*$^{-/-}$ mice showed increased adipocyte size relative to controls (**Fig. 1e,f**). A large amount of lipid accumulation in liver, skeletal muscle and brown adipose tissue (BAT) was observed in *Angptl6*$^{-/-}$ mice compared with *Angptl6*$^{+/-}$ and wild-type mice (**Fig. 1g**).

Metabolic disorders in *Angptl6*$^{-/-}$ mice

To address alternative causes of increased body weight in *Angptl6*$^{-/-}$ mice, we compared lipid metabolism, rectal temperature, basal metabolic rate and food intake of *Angptl6*$^{-/-}$ and wild-type mice. Significant increases were observed in serum cholesterol and free fatty acid (FFA) concentrations in *Angptl6*$^{-/-}$ mice, whereas there were no significant differences in serum triglyceride concentration between genotypes (**Fig. 2a**). *Angptl6*$^{-/-}$ mice also showed significant decreases in rectal temperature and whole-body oxygen consumption rates compared with wild-type mice (**Fig. 2b**). A small, statistically insignificant increase was observed in daily food intake in *Angptl6*$^{-/-}$ mice compared with controls (**Fig. 2b**).

Adipose tissue has a substantial influence on systemic glucose homeostasis through secretion of adipocytokines[2,16,17]. *Angptl6*$^{-/-}$ mice showed mild hyperglycemia and severe hyperinsulinemia (**Fig. 2c**). To investigate this point further, we performed intraperitoneal glucose and insulin tolerance tests (IGTT and IITT, respectively). Both hyperglycemia and hyperinsulinemia were detected in *Angptl6*$^{-/-}$ mice throughout the time course of the experiment